Tendon response to matrix unloading is determined by the patho-physiological niche

Stefania L. Wunderli[1,2]

Ulrich Blache[1,2]

Agnese Beretta Piccoli[1,2]

Barbara Niederöst[1,2]

Claude N. Holenstein[1,2]

Fabian Passini[1,2]

Unai Silván[1,2]

Louise Bundgaard[3]

Ulrich auf dem Keller[3]

Jess G. Snedeker[1,2]

[1] University Hospital Balgrist, University of Zurich, Switzerland

[2] Institute for Biomechanics, ETH Zurich, Switzerland

[3] Department of Biotechnology and Biomedicine, Technical University of Denmark, Denmark

April 2019

Address for Correspondence: Prof. Jess G. Snedeker
                                  Balgrist Campus
                                  Lengghalde 5
                                  CH - 8008 Zürich, Switzerland
                                  Tel.: 0041 44 510 73 30
                                  E-Mail: jess.snedeker@hest.ethz.ch

Author contributions:

Study concept and design: SLW, FP, US, JGS. Collection and/or assembly of data: SLW, UB, ABP, BN, LB. Data analysis: SLW, UB, CNH, UADK. Data interpretation and manuscript writing: SLW, UB, UADK, JGS.

1 **Abstract**

2   Aberrant matrix turnover with elevated matrix proteolysis is a hallmark of tendon pathology. While

3   tendon disease mechanisms remain obscure, mechanical cues are central regulators. Unloading of

4   tendon explants in standard culture conditions provokes rapid cell-mediated tissue breakdown. Here we

5   show that biological response to tissue unloading depends on the mimicked physiological context. Our

6   experiments reveal that explanted tendon tissues remain functionally stable in a simulated avascular

7   niche of low temperature and oxygen, regardless of the presence of serum. This hyperthermic and

8   hyperoxic niche-dependent catabolic switch was shown by whole transcriptome analysis (RNA-seq) to

9   be a strong pathological driver of an immune-modulatory phenotype, with a stress response to reactive

10   oxygen species (ROS) and associated activation of catabolic extracellular matrix proteolysis that

11   involved lysosomal activation and transcription of a range of proteolytic enzymes. Secretomic and

12   degradomic analysis through terminal amine isotopic labeling of substrates (TAILS) confirmed that

13   proteolytic activity in unloaded tissues was strongly niche dependent. Through targeted

14   pharmacological inhibition we isolated ROS mediated oxidative stress as a major checkpoint for matrix

15   proteolysis. We conclude from these data that the tendon stromal compartment responds to traumatic

16   mechanical unloading in a manner that is highly dependent on the extrinsic niche, with oxidative stress

17   response gating the proteolytic breakdown of the functional collagen backbone.

18 **Introduction**

19 Tendon is a highly specialized connective tissue that consists largely of sparsely distributed stromal

20 tendon fibroblasts in a collagen-rich extracellular matrix (ECM). The fact that tendons bear

21 physiologically extreme mechanical stresses is reflected by its tightly packed and highly structured

22 ECM. The load bearing tendon core is comprised by hierarchically organized type-I collagen fibrils,

23 fibres and fascicles (or fibre bundles) [1], with fascicles representing the basic functional load-bearing

24 unit of stromal tissue [2, 3]. Physiological mechanical signals are understood to regulate the lifelong

25 adaption of the tissue to individual functional demands [4-8], with a narrow gap between beneficial and

26 detrimental mechanical loads [9-12]. This threshold is often exceeded, with tendon disorders

27 accounting for 30 – 50% of all musculoskeletal clinical complaints associated with pain [13].

28 Our basic knowledge of the molecular and cellular mechanisms behind tendon physiology and

29 pathology is limited [14-16], yet damage and inadequate repair are considered to be central to tendon

30 disease onset and progression [17-19]. The stimuli that trigger tissue healing responses remain unclear,

31 potentially being a direct effect of cellular activation by overloading or by unloading after isolated fibre

32 rupture with subsequently altered cell-matrix interaction [20]. However, the mechanisms of

33 overloading and underloading may not be mutually exclusive, with tissue damage resulting in localized

34 regions of both load types. Regardless of the mechanism of damage activation, aberrant healing

35 processes typically result in a relatively disorganized and mechanically inferior repair tissue [21-23].

36 Tendinopathy severity is graded by its histopathological score, characterized by the extent of

37 disorganized collagen matrix, abnormal cell shape, presence of inflammation, increased cellularity,

38 vascularization and neuronal ingrowth [24-28]. These hallmarks of disease intimately involve tissue

39 turnover and proteolytic breakdown of the ECM [29-32]. Although pathological matrix turnover is

40 central to tendinopathy, very little is known about either the initiation or regulation of tissue catabolism

41 in the tendon core [33-36].

42 The healthy tendon stromal niche represents a low-oxygen and low-temperature tissue that is minimally

43 vascularized. Tendon fibroblasts reside in a state of relative metabolic quiescence compared to stromal

44 cells in other tissues [37]. Tendon repair thus likely involves closely coordinated interaction between

45 the hypovascularized intrinsic tendon core and the peritendinous synovial compartment of the tissue

46 that connects to the vascular, immune and nervous systems [38]. Although a clear picture is only

47 emerging, we speculate that mechanical sensors within the intrinsic tendon compartment recruit

48   structures of the extrinsic compartment resulting in neo-vascularization, neuronal ingrowth, immune

49   response and inflammation (Figure 1A) [38]. While patho-histological investigations of symptomatic

50   tendon phenotypes clearly demonstrate the presence of blood vessels within the tendon proper, it

51   remains unclear, which signalling-cascades are initiated in the intrinsic compartment by external

52   factors [39-42].
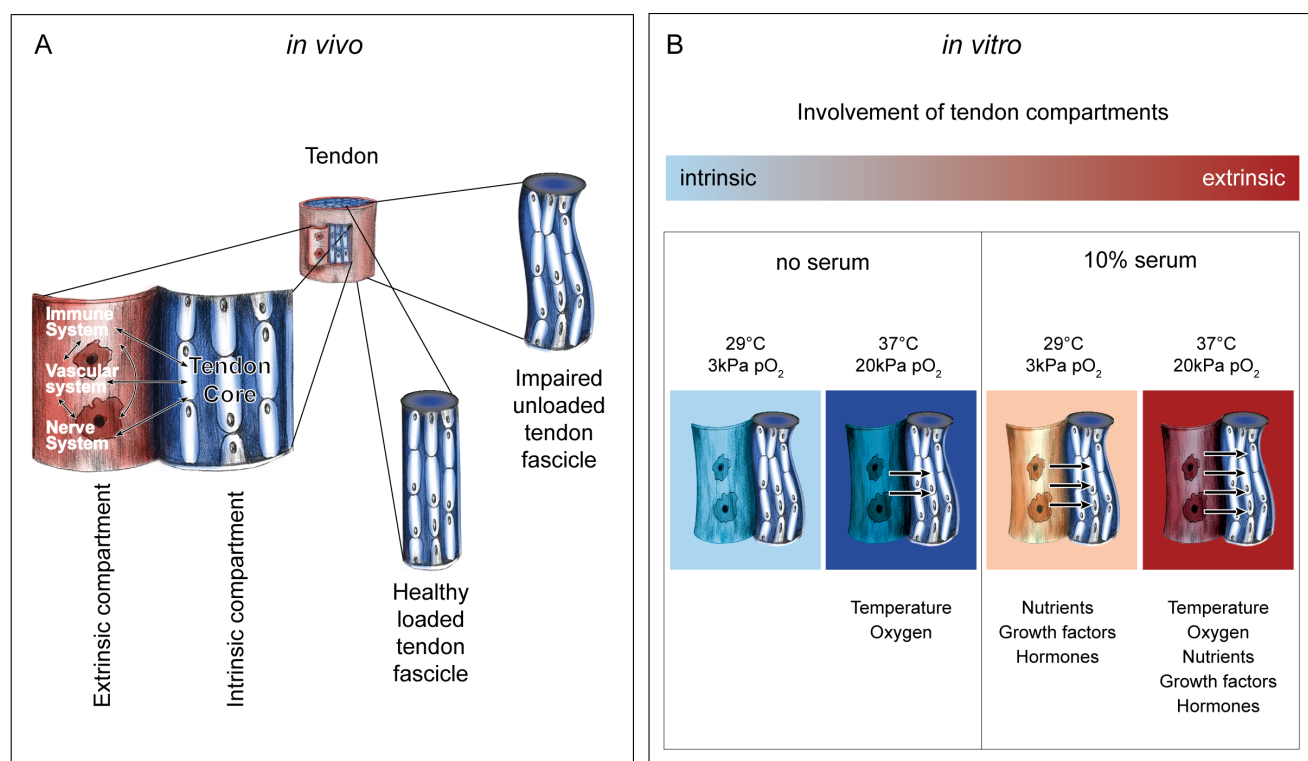
Figure 1: Tendon *in vivo* and *in vitro* model system. (**A**) Tendon is a hierarchically structured tissue. It mainly consists of densely packed collagen type I matrix and tendon cells (tenocytes) that are responsible for tissue maintenance. The tendon fascicle is the basic functional unit of the tendon (tendon core) and represents the intrinsic tendon compartment. The extrinsic compartment comprises the wrapping layer with synovium-like character that connects immune, vascular and nervous system. Wrapping layers are present at several hierarchical levels and are named endotendon, epitenon and paratenon (from lowest to highest level). It is thought that intrinsic and extrinsic compartments interact with each other at all levels to ensure proper tissue maintenance during homeostasis or repair. In a healthy homeostatic tissue tendon fascicles are loaded, while unloading of tendon fascicles may occur due to overloading and subsequent rupture of sub-tissue structures or upon immobilization. (**B**) In our *ex vivo* model the impaired tendon core is represented by an unloaded murine tail tendon fascicle. By varying temperature, oxygen and serum content of the culture conditions we mimicked the degree of involvement of the extrinsic compartment on the cell-driven healing process.

53 In this study we investigated how deviations from a low-oxygen, low-temperature tissue niche affect

54 resident stromal cells, specifically hypothesizing that the tissue niche is an important regulator of

55 cellular response to matrix damage. We established a system in which explanted murine tail tendon

56 fascicles served as a model of an independent unit of the intrinsic compartment that had been unloaded

57 by mechanical tissue damage. Unloaded tendon fascicles were exposed to different niches of varying

58 temperature, oxygenation and nutrient supply to mimic pathological and vascularized states of different

59 severity (Figure 1B). We compared mechanical properties, cell viability, metabolic activity, tissue

60 morphology, whole transcriptome, and protein degradomes and secretomes. Hereby we identified

61 mechanisms of extrinsic tendon compartment regulation on the response of intrinsic tendon cells

62 towards tissue homeostasis or pathologic tissue degeneration by activating an immune-related cellular

63 response, production of reactive oxygen species and downstream activation of proteolytic enzymes.

64

65 **Methods**

66 *Ex vivo* **tissue culture**

67 Tendon fascicles were extracted from tails of freshly euthanized 12-13 weeks old wild-type C57BL6/J

68 male mice. Tendon fascicles were gently isolated from each tail using a surgical clamp and distributed

69 among the control and treatment groups in a non-biased fashion. The explanted fascicles were

70 cultivated in absence of mechanical load and examined at designated time-points (6, 12, 18, 24 days).

71 Freshly isolated fascicles served as a positive tissue control (day 0). Devitalized fascicles were

72 generated by three freeze-thaw cycles before further use and served as negative control. Fascicles were

73 cultured in serum-free medium (high glucose Dulbecco's Modified Eagle's Medium (DMEM), 1% N2-

74 supplement (v/v), 1% penicillin-streptomycin (v/v), 200μM L-ascorbic acid phosphate magnesium salt

75 n-hydrate) or serum-supplemented medium (high glucose DMEM, 10% fetal bovine serum (v/v), 1%

76 penicillin-streptomycin (v/v), 1% non-essential amino acids (v/v), 200μM L-ascorbic acid phosphate

77 magnesium salt n-hydrate). Fascicles were maintained in a humidified atmosphere containing 5% CO_2

78 at either low oxygen partial pressure (pO_2 = 3kPa) and low temperature (29 °C) or high oxygen partial

79 pressure (pO_2 = 20kPa) and temperature (37°C). The fascicles in serum-supplemented medium were

80 additionally cultured in intermediate conditions at high oxygen and low temperature or vice versa.

81 Medium was changed every sixth day. All compounds of the cell culture media were purchased from

82 Sigma Aldrich, except for the ascorbic acid (Wako Chemicals) and the N2-supplement (Gibco). The

83 Cantonal Veterinary office of Zürich ethically approved all animal experiments (permit number

84 ZH265/14) and a total number of 40 mice was used.

85 Physiological tail tendon temperature of healthy mice was estimated by infrared-measurements of the

86 cutaneous tail temperature in 40 animals (Infrared thermometer 153-IRB, Bioseb).

87

88 **Biomechanical testing and analysis**

89 Force-displacement data were recorded on a custom-made uniaxial stretch device as previously

90 described [43]. In brief, fascicles were clamped, pre-loaded to 0.015N (corresponding to 0% strain) and

91 preconditioned to 1% strain with five stretch cycles (n=6, independent samples from different mice).

92 The tangential elastic-modulus was calculated in the linear part of the stress-strain curve (0.5 – 1%

93 strain) of a single additional stretch cycle to 1% by fitting a linear slope (Matlab R2016a, Version

94 9.0.0.341360). The pre-load was reapplied after every cycle. Nominal stress was calculated based on

95 the initial cross-sectional area. Cross-sectional area was determined from the diameter assuming a

96 round specimen shape. Diameter was measured using automated evaluation of microscopic images

97 (Matlab R2016a, Version 9.0.0.341360), which were recorded before the treatment at three different

98 locations along the fascicle with a 20-fold magnification (Motic AE2000, Plan LWD 20x, WD 4.7).

99

100 **Cell viability and ATP measurements**

101 Dead cells in the fascicles were stained with Ethidium Homodimer-1 (2μM, AS 83208, Anaspec)

102 previous to 10% formalin fixation (HT5011, Sigma Aldrich). Subsequently, cell nuclei were stained

103 with NucBlue reagent (1 drop/ml = ca. 10μl, R37606, Thermo Fischer, Switzerland) and embedded in a

104 50% Glycerol:PBS solution. Z-stack fluorescent images were obtained in triplicates by using a

105 spinning disc confocal microscope (iMic, FEI) equipped with a Hamamatsu Flash 4.0 sCMOS camera

106 and a SOLE-6 Quad laser (Omicron) and using a 20x objective (Olympus, UPLSAPO, N.A. 0.75).

107 Total number of imaged cells, percentage live cells (total cell number minus dead cells) and fascicle

108 volume (n=6, independent samples from different mice) were assessed by means of a custom

109 microscopic image analysis tool (MATLAB, R2016a 9.00.34160). Number of cells was determined in

110 a measurement depth of 60μm (from surface) and the volume of the circular segment was calculated by

111 measuring length and diameter of total specimen z-projection.

112 ATP was assessed by using a luminescence based ATP detection assay according to the manufacturer's

113 instructions (CellTiterGlo3D, G9681, Promega). ATP standards were prepared from a 10mM stock

114   solution (P1132, Promega). After ATP measurement the 20mm long fascicle parts (n=4 in duplicate

115   measurements, two fascicles per animal) were frozen at -80°C and subsequently digested at 56°C

116   overnight by Proteinase K (10mM in Tris-HCl, 19133, Qiagen). To account for potentially differential

117   cell proliferation rate between treatments all the ATP quantifications were normalized to DNA content

118   in the same samples. The quantity of DNA in each digest was measured by fluorescent signal detection

119   using the Quant-iT™ dsDNA High-Sensitivity Assay Kit (Q33232, Thermo Fisher) according to the

120   manufacturer's protocol. Whole fascicles were cut to equally sized parts (20mm), while one half was

121   processed and measured directly after isolation (day 0) and the other half after the treatment (day 6 and

122   12). Lumiescence and fluorescence were both recorded on a microplate reader (SpectraMAX Gemini

123   XS).

124

125   **Second harmonic generation imaging and transmission electron microscopy of tendon fascicles**

126   Collagen was visualized by second harmonic generation (SHG) imaging of whole mount tissues on a

127   multi-photon and confocal fluorescence microscope (Leica TCS SP8) equipped with photon-counting

128   hybrid detectors and an ultrafast near infrared laser (Insight DS+ Dual, Spectra Physics) using 25x

129   magnification (HC IRAPO L 25x, NA 1.0), an excitation wavelength of 880nm and a SHG-compatible

130   fluorescence filter cube (440/20 & 483/32 with 455 SP). Cell nuclei were imaged from the same

131   samples. All the samples were recorded at the same laser power and gain control with a z-step size of

132   0.3μm. After image acquisition 70 stacks were z-projected using ImageJ (Fiji, NIH Version 1.0).

133   For transmission electron microscopy whole mouse tail tendon fascicles were fixed in 2.5%

134   glutaraldehyde (G5882, Sigma-Aldrich) in 0.1M Cacodylat buffer (pH 7.2) for 20 minutes. To

135   visualize the collagen fibrils, samples were contrasted with 1% uranyl acetate in water for 1 h. All

136   samples were then dehydrated with graduated concentration of ethanol and propylene oxide. Specimens

137   were infiltrated and embedded in Epon (polymerized at 60 °C for 48 h). Ultra-thin longitudinal and

138   cross sections were cut with a diamond knife and mounted on uncoated grids. Samples were then

139   imaged with a transmission electron microscope (TEM-FEI Tecnai G2 Spirit).

140

141   **RNA sequencing**

142   For each experimental group 16-20 fascicles were pooled after 6 days of culture, snap frozen in liquid

143   nitrogen and pulverized in QIAzol lysis reagent (#79306, Qiagen) by cryogenic grinding (FreezerMill

144   6870, SPEX™SamplePrep). Tissue lysates were mixed with 1-bromo-3-chloropropane (B9673, Sigma-

145   Aldrich) at a ratio of 1:4 and the RNA containing aqueous/organic phase was separated using 5Prime

146   PhaseLock Gel Heavy (#2302830, LabForce). RNA was extracted by using the RNeasy micro Kit

147   (74004, Quiagen). The quantity and quality of the isolated RNA (n = 3, independent pools of fascicles

148   from different mice) was determined with a Qubit® (1.0) Fluorometer (Life Technologies, California,

149   USA) and a Bioanalyzer 2100 (Agilent, Waldbronn, Germany). The TruSeq Stranded mRNA Sample

150   Prep Kit (Illumina, Inc, California, USA) was used in the succeeding steps. Briefly, total RNA samples

151   (100 ng) were poly-A selected and then reverse-transcribed into double-stranded cDNA with

152   Actinomycin added during first-strand synthesis. The cDNA sample was fragmented, end-repaired and

153   adenylated before ligation of TruSeq adapters. The adapters contain the index for multiplexing.

154   Fragments containing TruSeq adapters on both ends were selectively enriched with PCR. The quality

155   and quantity of the enriched libraries were validated using Qubit® (1.0) Fluorometer and the

156   Bioanalyzer 2100 (Agilent, Waldbronn, Germany). The product is a smear with an average fragment

157   size of approximately 360 bp. The libraries were normalized to 10nM in Tris-Cl 10 mM, pH8.5 with

158   0.1% Tween 20. The TruSeq SR Cluster Kit v4-cBot-HS (Illumina, Inc, California, USA) was used for

159   cluster generation using 8pM of pooled normalized libraries on the cBOT. Sequencing were performed

160   on the Illumina HiSeq 4000 single end 125 bp using the TruSeq SBS Kit v4-HS (Illumina, Inc,

161   California, USA).

162

163   **RNA sequencing data analysis**

164   Bioinformatic analysis was performed using the R package ezRun[1] within the data analysis framework

165   SUSHI [44]. In details, the raw reads were quality checked using Fastqc[2] and FastQ Screen[3]. Quality

166   controlled reads (adaptor trimmed, first 5 and last 6 bases hard trimmed, minimum average quality

167   Q10, minimum tail quality Q10, minimum read length 20nt) were aligned to the reference genome

168   (Ensembl GRCm38.p5) using the STAR aligner [45]. Expression counts were computed using

169   featureCounts in the Bioconductor package Subread [46]. Differential expression analysis was

170   performed using the DESeq2 package [47], where raw read counts were normalized using the quantile

171   method, and differential expression was computed using the quasi-likelihood (QL) F-test[4]. Gene

172   ontology (GO) enrichment analysis was performed using Bioconductor packages goseq [48] and

---

[1] https://github.com/uzh/ezRun
[2] http://www.bioinformatics.babraham.ac.uk/projects/fastqc/
[3] http://www.bioinformatics.babraham.ac.uk/projects/fastq_screen/
[4] https://bioconductor.org/packages/devel/bioc/manuals/DESeq2/man/DESeq2.pdf

173   GOStats [49]. Quality checkpoints [50], such as quality control of the alignment and count results,

174   were implemented in ezRun and applied through out the analysis workflow to ensure correct data

175   interpretation. Differentially expressed genes were considered at a p-value < 0.05 and a log2ratio > 1.

176   Pathway analyses were performed using MetaCore database via GeneGo tool from Thomson Reuters[5]

177   and the Kyoto Encyclopedia of Genes and Genomes (KEGG) database.

178

179

180   **Detection of reactive oxygen species**

181   To quantify the production of reactive oxygen species (ROS) tendon fascicles (n=6, independent

182   samples from different mice) were stained with 2′,7′-Dichlorofluorescin diacetate (DCFH-DA, D6883,

183   Sigma Aldrich). Control fascicles and cultured fascicles were incubated for 30 minutes with 50µM

184   DCFH-DA in PBS at either 29°C, 3kPa pO_2 or 37°C, 20kPa pO_2 at day 0 and day 6 according to the

185   previous culture. Immediately after incubation, fluorescence was recorded by acquiring z-stacks at

186   steps of 1µm through the whole fascicles depth at an emission wavelength of 488nm on the spinning

187   disc confocal microscope setup as described above using a 10x objective (Olympus, UPLSAPO, N.A.

188   0.4). Quantification of fluorescent signal reflected from the tissue was evaluated by measuring

189   cumulative mean intensity of z-projections using ImageJ (Fiji, NIH Version 1.0). Images were taken in

190   triplicates.

191

192   **Quantitative real-time polymerase chain reaction (qRT-PCR)**

193   RNA was extracted as described above but using the PureLink[TM] RNA Micro Scale Kit (#12183016,

194   Invitrogen). cDNA was prepared by reverse transcribing 99ng total RNA in a volume of 44µl using the

195   High-Capacity RNA-to-cDNA™ Kit (#4387406, Applied Biosystems). qRT-PCR was carried out

196   using 2µl cDNA, 5µl TaqMan Universal Master Mix, 0.5µl TaqMan Primer (Applied Biosystems) and

197   2.5µl RNase free water. Samples were amplified in 40 cycles on a StepOnePlus[TM] thermocycler

198   (Applied Biosystems) and reactions were run in technical duplicates. Following primers were used:

199   Mm00442991_m1   (*MMP9*),   Mm01168399_m1   (*MMP10*),   Mm00439491_m1   (*MMP13*),

200   Mm01310506_m1 (*Ctsb*), Mm00515580_m1 (*Ctsc*), Mm00515586_m1 (*Ctsd*), Mm01255859_m1

201   (*Ctss),* Mm00517697_m1 (*Ctsz*). Relative gene expression was calculated by the comparative Ct

---

[5] https://portal.genego.com/

202   method [51] by normalizing the data to the stable housekeeping gene Mm0129059_m1 (*Anxa5*) and to

203   freshly isolated samples.

204

Inhibition experiments

206   Tendon fascicles were cultured under degrading conditions (serum, 37°C and 20kPa pO$_2$) for 12 days.

207   From the beginning of the incubation time medium was supplemented with the ROS inhibitor Tempol

208   (4-hydroxy-2,2,6,6-tetramethylpiperidin-1-oxyl)) (1mM, 176141-1G, Sigma), the collagenase inhibitor

209   Ilomastat   ((*R*)-*N*′-Hydroxy-*N*-[(S)-2-indol-3-yl-1-(methylcarbamoyl)ethyl]-2-isobutylsuccinamide)

210   (25µM, CC1010, Merck Millipore) or a combination of both. Medium with DMSO (#472301, Sigma)

211   was used as a control. Culture medium was changed after 6 days. Tissue stiffness was measured at day

212   0 and day 12 and negative control fascicles were devitalized as described above.

213

Mass spectrometry-based proteomics

215   Terminal amine isotope labeling of substrates (TAILS) analysis, whereby protein N-termini were

216   enriched from 12 day cultures of mechanically intact and impaired fascicles, was performed according

217   to the previously described protocol [52] except for using 10plex Tandem mass Tag^{TM} labelling (TMT,

218   #90110, Thermo Fisher) and adding the trypsin at a ratio of 1:20 (trypsin/protein ratio). Prior to protein

219   denaturation and labelling, proteins of samples were extracted by pressure cycling technology (60

220   cycles of 45'000psi for 20s, atmospheric pressure for 10s, 33°C) from ca. 4mg tissue in a buffer

221   containing 4M Guanidine hydrochloride (Sigma-Aldrich), 250mM HEPES (Sigma-Aldrich (pH 7.8)

222   and protease inhibitor cocktail (cOomplete EDTA-free, Roche) using a Barocycler 2320ETX (Pressure

223   Biosciences Inc.) (Figure 6A).

224   Secretomes of 18-22 equally sized and 12-days-cultured fascicles were collected for each of the two

225   conditions in 2ml serum-free and phenol red-free DMEM (#31053028, Gibco supplemented with 1%

226   penicillin-streptomycin (v/v), 200µM L-ascorbic acid phosphate magnesium salt n-hydrate and 1%

227   GlutaMAX (v/v), A1286001, Gibco) during an exposure time of 48 hours. Fascicles were thoroughly

228   washed with PBS before secretome collection. Secretomes were supplemented with protease inhibitor

229   cocktail (cOomplete EDTA-free, Roche) and concentrated ca. 40 times by centrifugal filtration (3K

230   Amicon Ultra, Merck Millipore, 14'000g, 4°C) and buffer was exchanged to 4M Guanidine

231   hydrochloride in 50mM HEPES (pH 7.8). Subsequently, secretomes were reduced in tris(2-

232   carboxyethyl)phosphine (200mM , Sigma-Aldrich) and alkylated in chloroacetamide (400mM, Sigma-

233   Aldrich) for 30 minutes at room temperature and then digested by LysC (Lysyl endopeptidase, #125-

234   05061, Wako, ratio LysC/protein 1:100) and trypsin (Trypsin Gold, V5280, Promega, ratio

235   trypsin/protein 1:20) overnight. Desalting was performed according to the TAILS protocol [52].

236   PreTAILS, TAILS and secretome peptide mixtures were loaded onto an PepMap100 C18 precolumn

237   (75 µm x 2 cm , 3µm, 100Å, nanoViper, Thermo Scientific) and separated on a PepMap RSLC C18

238   analytical column (75 µm x 50 cm , 2µm, 100Å, nanoViper, Thermo Scientific) using an EASY-nLC™

239   1000 liquid chromatography system (Thermo Scientific) coupled in line with a Q Exactive mass

240   spectrometer (Thermo Scientific). Separation of 1 µg of peptide mixture was achieved by running a

241   constant flow rate of 250 nL/min in 0.1% formic acid/99.9% water and a 140 min gradient from 10% to

242   95% (23% for 85min, 38% for 30min, 60% for 10min, 95% for 15min) elution buffer (80%

243   acetonitrile, 0.1% formic acid, 19.9% water). A data-dependent acquisition (DDA) method operated

244   under Xcalibur 3.1.66.10 was applied to record the spectra. The full scan MS spectra (300-1750 m/z)

245   were acquired with a resolution of 70,000 after accumulation to a target value of 3e6. Higher-energy

246   collisional dissociation (HCD) MS/MS spectra with fixed first mass of 120 m/z were recorded from the

247   10 most intense signals with a resolution of 35,000 applying an automatic gain control of 1e6 and a

248   maximum injection time of 120ms. Precursors were isolated using a window of 1.6 m/z and fragmented

249   with a normalized collision energy (NCE) of 28%. Precursor ions with unassigned or single charge

250   state were rejected and precursor masses already selected for MS/MS were excluded for further

251   selection for 60s. Settings for the scan of the secretome peptide mixture were the same except for using

252   a resolution of 17,500 for recording the MS/MS spectra, a maximum injection time of 60ms, and a

253   NCE of 25%.

254

255   **Proteomics data analysis**

256   Raw data files were analysed using Proteome Discoverer™ 2.3 software (PD) searching the peak lists

257   against a database collated in the UniProt reference proteome for the species *Mus musculus* (ID: 10090,

258   entries: 17'005). Search parameters for the TAILS experiment were set according to the previously

259   published protocol [52], treating preTAILS and TAILS samples as fractions. For protein-level analysis,

260   quantifiable internal fully tryptic peptides and mature protein N termini were annotated with help of

261   TAILS-Annotator [53], extracted from PD peptide groups and their normalized, scaled abundances

262   were summed up per corresponding protein. The resulting list was curated for protein FDR<0.01 based

263   on PD protein analysis and proteins with significantly differential abundance between conditions

264   determined applying limma moderated t-statistics with Bonferroni-Hochberg multiple testing

265   correction in CARMAweb [54]. Similarly, quantifiable N-terminal peptides were extracted from the

266   PD analysis, annotated using TopFIND [55] and analysed for statistically differential abundance using

267   CARMAweb applying the same parameters as for proteins based on scaled abundances summed up per

268   stripped peptide sequence. Volcano plots were generated using GraphPad Prism (GraphPad Software

269   8.0).

270   Raw data files of the secretome experiments were processed by PD using the label-free quantification

271   algorithm Minora Feature Detector node and proteins tested for differential abundance between

272   conditions applying limma moderated t-statistics using CARMAweb [54] on normalized scaled

273   abundance values exported from PD.

274

275   **Statistics**

276   RStudio (Version 1.1.423, 2016, Boston, MA) was used for statistical tests and graph illustrations [56].

277   Mean values of elastic moduli were compared by one-way analysis of variance (ANOVA) followed by

278   contrast analysis. Additionally, multiple linear regression analysis was used to assess the linear

279   relationship between culture time-points, temperature, oxygen and serum as predictors for the response

280   variable elastic modulus. Temperature, oxygen and serum were coded as $0 = 29°C$ / $3kPa$ O_2 / no serum

281   and $1 = 37°C$ / $20kPa$ O_2, / 10% serum, respectively. Non-parametric data (percentage live cells, total

282   cell number, ATP measurement, qRT-PCR, DCFH-DA measurement) was analysed by means of the

283   Mann-Whitney U test to probe for differences between two treatment groups. Results were considered

284   to be statistically significant with * at p-values < 0.05, ** < 0.01 and *** < 0.001. Further information

285   on individual statistical tests is available in the respective figure legends.

286

287 **Results**

288 **Mechanical properties of tendon fascicles are impaired by *ex vivo* culture conditions mimicking**

289 **vascularization**

290 To investigate the impact of extrinsic tissue factors on underload-induced alterations in tendon core

291 mechanical properties we established a tendon explant model. Intact tendon fascicles were isolated

292 from murine tails and cultured deprived from load to mimic tendon underloading after damage. We

293 cultured the tendon fascicles with or without serum and under varying temperature and oxygen levels

294 to study the involvement of extrinsic factors associated with vascularization under tightly controlled

295 conditions (Figure 1B). Fascicles cultured in serum-free medium, at low oxygen partial pressure (3kPa

296 pO_2) and low temperature (29 °C) mimic a quiescent, minimally nourished tissue that is typical of the

297 tendon core within a healthy tissue [57-59] (Supplementary figure S1). In contrast, a pathologically

298 vascularised tissue was mimicked by elevated temperature, oxygen and nutrients (37°C, 20kPa pO_2,

299 10% serum) that would follow upon involvement of blood vessels and synovial tissue.

300

301 High tensile strength and high elastic modulus characterize a functional tendon, allowing it to transmit

302 muscle forces across joints of the body. To evaluate the effect of tissue culture niche on tendon

303 integrity we measured the elastic moduli of tendon fascicles after 6, 12, 18 and 24 days (d6 – d24).

304 Elastic moduli were calculated from force-displacement curves that were recorded on a custom-made

305 uniaxial test device [43]. The elastic modulus of freshly isolated (uncultured) fascicles was 1300 MPa

306 (sd: 242 MPa). Under serum-free conditions, the elastic moduli were not affected by load-deprived

307 culture and remained stable independent of oxygen partial pressure and temperature throughout the

308 experimental period (Figure 2A, 2B). Likewise, including serum to the low temperature (29°C) and low

309 oxygen (3kPa pO_2) condition did not alter emergent mechanical properties (Figure 2C). In contrast, the

310 elastic modulus was strongly and significantly decreased when maintaining the tendon fascicles under

311 conditions that mimic a pathologically vascularized tendon niche (37°C, 20kPa pO_2, 10% serum)

312 (Figure 2D). Here, the elastic modulus started to decrease after day 6 and dropped to 367 MPa (sd: 426

313 MPa) at day 18. At day 24, we were not able to measure the elastic modulus due to a complete loss of

314 load bearing capacity. Notably, the decrease of mechanical properties did not occur in devitalized

315 control tendons, indicating that intrinsic cellular processes and not proteolytic activity of serum

316 components were responsible for the decrease in elastic modulus (Supplementary figure S2).

317   Oxygen- and temperature-dependent losses of mechanical properties in the serum-containing

318   environment happened in an additive manner, whereby low oxygen (37°C, 3kPa pO_2) and low

319   temperature (29°C, 20kPa pO_2) each slowed the loss of mechanical properties (Supplementary figure

320   S3). Multiple linear regression analysis was carried out to investigate whether culture time-point,

321   temperature, serum and oxygen predict the elastic modulus of explanted tendon fascicles. A significant

322   regression equation was found (F(6, 127), 5.494, p = $4.37*10^{-5}$) with an R^2 of 0.21. Culture time-point

323   (β of d12 = -200.1, p = 0.02, β of d18 = -195.8, p = $6.2*10^{-4}$, β of d24 = -255.4, p = $6.3*10^{-3}$),

324   temperature (β = -284.5, p = $2.89*10^{-5}$) and oxygen (β = 163.26, p = 0.013) significantly predicted the

325   elastic modulus. Serum was not a significant predictor (β = -49.15, p < 0.45).

326   In summary, we established a novel *ex vivo* tendon model that represents different levels of extrinsic

327   compartment involvement during underload-mediated tendon remodelling. The model reveals that cell-

328   mediated processes drive loss of mechanical properties of the tendon fascicles at activating *ex vivo*

329   conditions (high levels of oxygen and temperature).
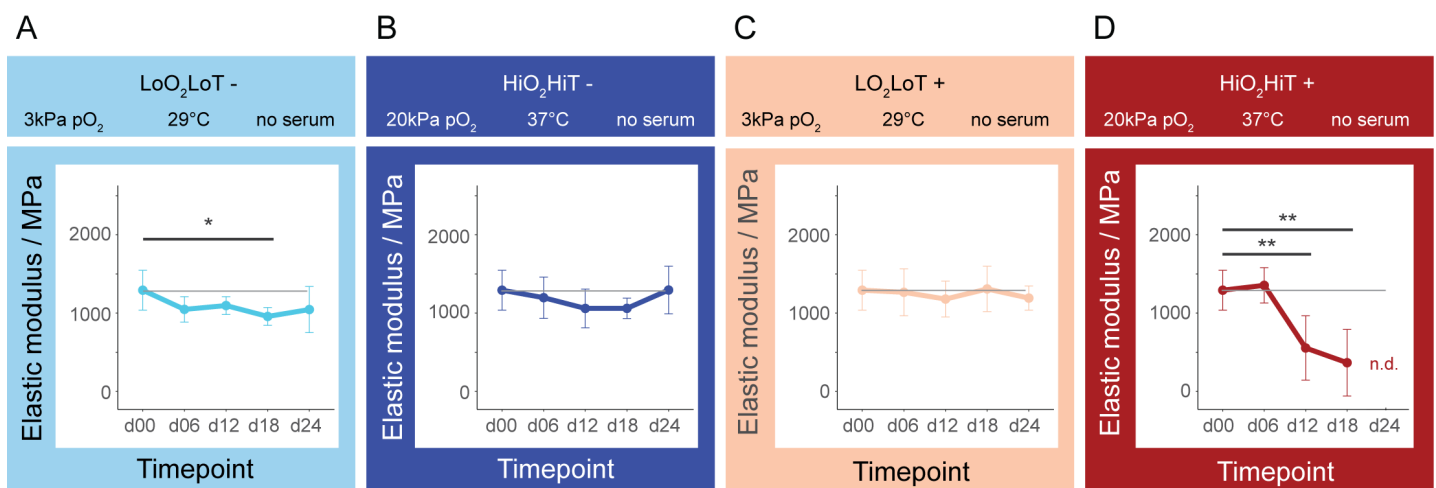
Figure 2: Elastic moduli of tendon fascicles cultured in different environments during 24 days (d24). The models represent increased involvement of the extrinsic compartment associated with vascularization of the tendon (**A** to **D**). Loss of mechanical properties only occurred under standard cell culture conditions in serum-supplemented medium, at a temperature of 37°C and atmospheric oxygen level (**D**). The data points represent mean values and the error bars are standard deviation. Statistical analysis was performed using one-way ANOVA followed by contrast analysis in RStudio. Mean values of each time-point (d06 – d24) were compared to the freshly isolated control (d00) within each condition (n = 6 independent samples from different mice, p-values: * < 0.05, ** < 0.01).

330 **Comparable cell viability, metabolism and gross ECM structure between functionally impaired**

331 **and intact tendon fascicles**

332 Loss of mechanical properties in a serum-supplemented environment is driven by high temperature and

333 oxygen in a cell-dependent manner. To gain deeper insights into the cellular processes that are

334 responsible for loss of mechanical properties we followed up on the intact and functionally impaired

335 groups. We therefore cultured the tendon fascicles at either low oxygen and low temperature

336 (LoO$_2$LoT+) or high oxygen and high temperature (HiO$_2$HiT+) in the presence of serum for the

337 following investigations.
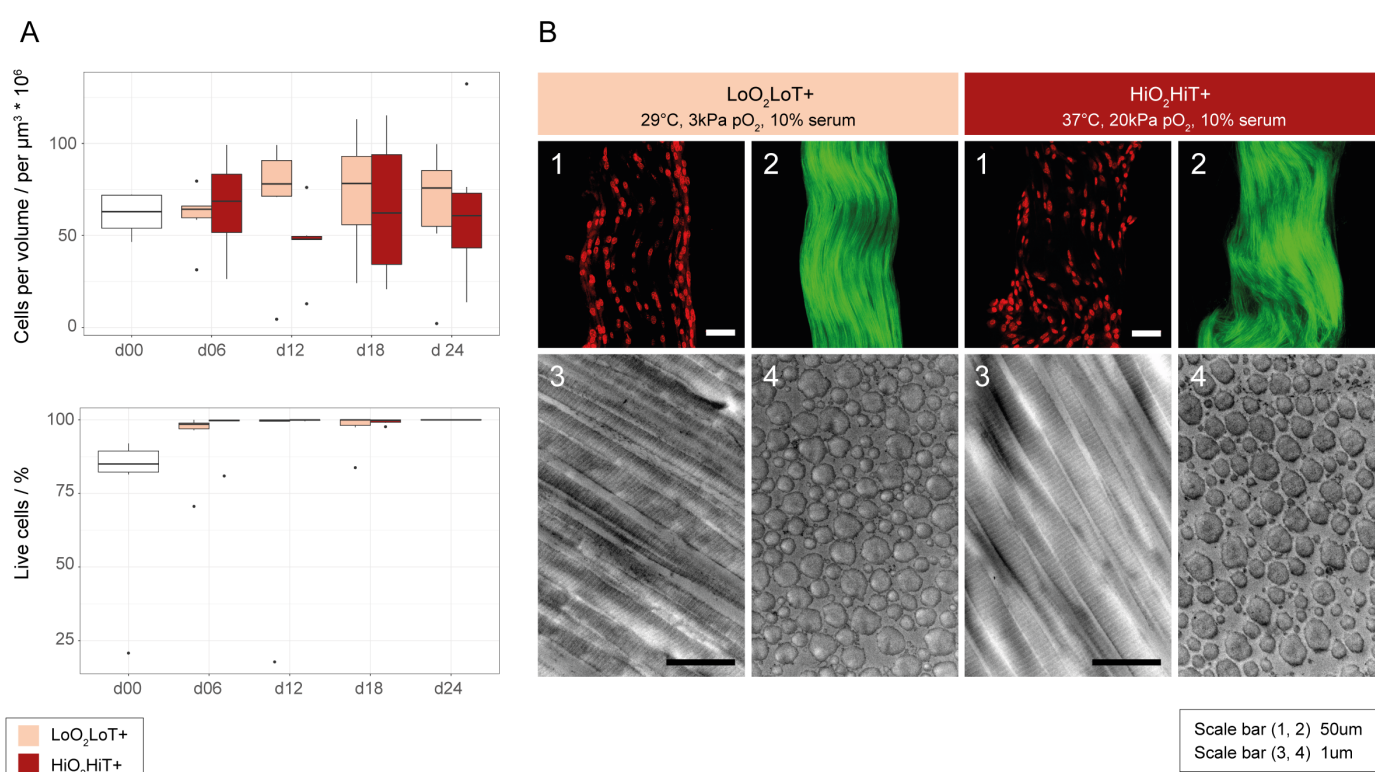
Fig. 3: Cell viability and morphological characterization of mechanically intact and impaired tendon fascicles. (A) Total cell number per volume (upper) stayed constant over time and cell viability (lower) was not significantly different between the HiO$_2$HiT+ and the LoO$_2$LoT+ group at any time-point. Single dead peripheral cells were always present in the d0 condition, which most probably died from shear forces occurring during the isolation process. However, these cells disappeared upon culture in serum, which explains the slightly lower percentage of live cells in the d0 condition. Statistical analysis was performed using Mann-Whitney U test in RStudio comparing the "LoO$_2$LoT+" to the "HiO$_2$HiT+" condition within each time point (d06 – d24) (n = 6, independent samples from different mice). (B) Tissue morphology after a treatment period of 12 days. (1) Second harmonic generation imaging and (2) nuclear shape of mouse tail tendon fascicles treated at either low oxygen and low temperature with serum (LoO$_2$LoT+) or high oxygen and high temperature with serum (HiO$_2$HiT+). (3) Transmission Electron Microscopy images in longitudinal and (4) transverse sections. Scale bars represent 50μm in the upper fluorescence images and 1um in the electron micrographs.

338   To evaluate whether cell number or viability contributed to altered mechanical properties we performed

339   a fluorescence-based cell viability assay in tendon fascicles after 6, 12, 18 and 24 days of culture. Total

340   cell number and cell viability within the tissue were not markedly different between the two conditions

341   as well as compared to the freshly isolated control tissue (Figure 3A). Further, metabolic activity as

342   measured by ATP concentration normalized to DNA content increased similarly in both culture

343   conditions after 6 and 12 days of culture compared to the freshly isolated control measured at day 0

344   (Supplementary figure S4). To investigate tendon fascicle morphology, we looked at macroscopic

345   alterations and additionally performed second harmonic generation imaging of collagen. In both

346   conditions, fascicles showed length contraction over time. Although fascicles in the HiO$_2$HiT+

347   environment contracted at earlier timepoints compared to the LoO$_2$LoT+ group, collagen fibres

348   appeared microscopically similar in both conditions (Figure 3B). Furthermore, also the ultra-structure

349   of collagen fibrils was qualitatively comparable between both groups as revealed by transmission

350   electron microscopy (Figure 3B).

351   Taken together, our data show that the loss of mechanical properties does not correlate with

352   pronounced changes at the cell or tissue matrix level. Therefore, we next aimed at investigating

353   changes that take place at the molecular level.

354

355   **Mechanical impairment is associated with strong transcriptome changes related to immune**

356   **system response, oxidative-stress, lysosome activation and proteolysis**

357   To investigate the molecular changes that are involved in the loss of mechanical properties we

358   compared the functionally impaired (HiO$_2$HiT+) and intact (LoO$_2$LoT+) tendon fascicles by

359   transcriptome analysis using RNA sequencing (RNA-seq). Overall we detected 23'675 known

360   transcripts according to the murine reference genome. Filtering revealed 3305 differentially expressed

361   genes (DEG) between the two groups, among which 1854 were up-regulated and 1451 were down-

362   regulated in the functionally impaired fascicles (Figure 4A and supplementary table ST1). To

363   systematically investigate their relationships, we functionally enriched all the DEGs within the gene

364   ontology (GO) Biological Process. Overrepresented GO terms mainly include immune-related

365   processes (Supplementary table ST2), whereof nearly 50% are additionally represented in the GO

366   enrichment of only up-regulated genes (Supplementary table ST3). Furthermore, we mapped all DEGs

367   onto the most relevant pathways via statistical enrichment analysis using the MetaCore database by
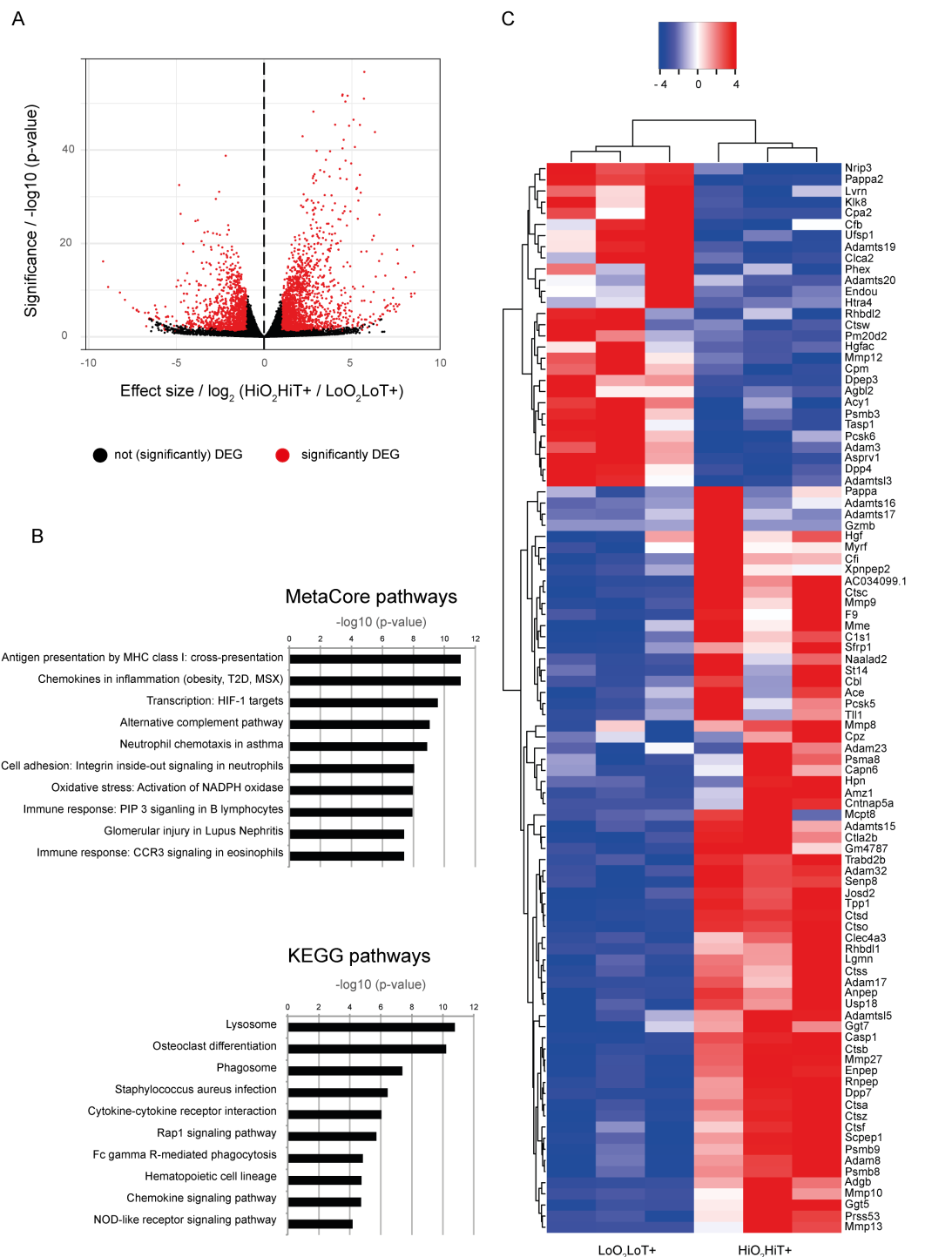
Figure 4: Transcriptome analysis of differentially expressed genes in mechanically intact vs. impaired tendon fascicles. (**A**) Volcano plot of differentially expressed genes between tendon fascicles cultured in HiO_2HiT+ and LoO_2LoT+. Genes coloured in red are considered as differentially expressed (DEG) and have a $\log_2$(fold change) > 1 and a significance of $p < 0.05$. (**B**) The top 10 enriched signalling pathways in the HiO_2HiT+ group compared to the LoO_2LoT+ group (determined by the MetaCore from GeneGo and KEGG database using both, up- and down-regulated genes). MHC = Major Histocompatibility Complex, T2D = Type 2 Diabetes, MSX = Metabolic Syndrome X (**C**) Unsupervised hierarchical clustering of differentially expressed genes in the LoO_2LoT+ and the HiO_2HiT+ group (n=3, independent pools of fascicles from different mice). Depicted are the DEGs with cut-off values of $\log_2$ ratio > 1 and $p < 0.05$. The clustering separates the genes by colour with positive or negative row-scaled Z-scores represented in red and blue, respectively.

368   GeneGo. The 10 most significantly altered pathways are shown in Figure 4B. Strikingly, 7 out of 10

369   pathways are related to immune system activation including professional phagocytic cells, such as

370   neutrophils, macrophages and dendritic cells. In addition, three identified pathways ("Chemokines in

371   inflammation", "HIF-1 target transcription" and "Activation of NADPH oxidase") are closely linked to

372   oxidative-stress-dependent processes (Figure 4B). The induced oxidative-stress related genes mainly

373   include regulatory proteins or subunits of the NADPH oxidase (NOX2/gp91^{phox}, p22^{phox}, p47^{phox},

374   p67^{phox}, p40^{phox}, Rac2, Vav1, Vav3), a transmembrane protein that catalyzes the production of

375   superoxide in different cell types (Supplementary figure S5A). All of these genes were significantly up-

376   regulated in the HiO$_2$HiT+ group.

377   Alternatively, we enriched all DEGs in the Kyoto Encyclopedia of Genes and Genomes (KEGG)

378   domain. One half of the top 10 identified gene pathways is associated with inward vesicular trafficking

379   destined to degradation in the lysosome ("Lysosomes", "Phagosomes", "Fc gamma R-mediated

380   phagocytosis", "Staphylococcus aureus infection", "NOD-like receptor signaling pathway") (Figure

381   4B). The lysosome is the main catabolic subcellular organelle responsible for degradation of

382   extracellular and intracellular components. Furthermore, "Osteoclast differentiation" suggests initiation

383   of a process that is relevant in ECM resorption as shown by up-regulation of the genes PPARG, CSF-1,

384   PI3K, RANK (TNFRSF11A) and RANKL (TNFSF11) and others (Supplementary figure S5B). The

385   KEGG pathway analysis including only up-regulated DEGs is mostly consistent with the analysis

386   including both, up- and down-regulated genes (Supplementary figure S5C).

387   Because we previously showed that tendon fascicles in the HiO$_2$HiT+ condition lose mechanical

388   properties, which most likely involves ECM breakdown, and due to the fact that pathway analysis of

389   DEGs suggests lysosomal degradation as a main process, we examined the GO term "proteolysis"

390   (GO:0006508). Indeed, we found 96 DEGs to be annotated to "proteolysis" of which 67 were up-

391   regulated in the HiO$_2$HiT+ (Figure 4C). Among them we found various extracellular proteases such as

392   matrix metalloproteinases (MMP 8, 9, 10, 13, 27), intracellular proteases involved in lysosomal

393   degradation such as cathepsins (cathepsin A, B, C, D, F, O, S, Z), and proteasome-related proteins

394   (PSMA 8, PSMB 3, 8, 9,).

395   In summary, the results reveal that the transcriptome changes between the mechanically intact

396   (LoO$_2$LoT+) and the mechanically impaired (HiO$_2$HiT+) group involve proteolysis, oxidative-stress-

397   related processes, immune system activation and lysosome involvement. These molecular changes are

398   all accompanied by a functional loss of fascicle mechanics.

Tendon mechanical integrity is rescued by inhibiting reactive oxygen species and proteases

Based on the experimental design (difference in temperature and oxygen saturation between the two groups) and the up-regulated oxidative stress-related pathways we hypothesized that reactive oxygen species (ROS) contribute to ECM degradation and loss of tendon mechanical properties as main regulators. To confirm ROS production we measured fluorescence of dichlorofluorescein (DCF), which is produced by intracellular oxidation upon esterase cleavage of the cell-permeable 2'-7'-Dichlorodihydrofluorescein diacetate (DCFH-DA). ROS were significantly increased in the functionally impaired (HiO$_2$HiT+) compared to the intact (LoO$_2$LoT+) tendon fascicles, confirming the RNA-seq findings on the tissue level (Supplementary figure S6).

Next, based on our RNA-seq data we hypothesised that ROS and MMPs are involved in the process of tendon fascicle degeneration. Therefore, we assessed the effects of ROS scavenging (Tempol) and MMP inhibition (Ilomastat) in the functionally impaired (HiO$_2$HiT+) condition over a time period of 12 days. Separate inhibition of ROS and MMPs partially protected against loss of mechanical properties as measured by the elastic moduli (Figure 5A). Therefore, we also investigated the combined effects of inhibiting both ROS and MMPs. Intriguingly, combined inhibition of ROS and MMPs resulted in complete maintenance of elastic modulus at levels of freshly isolated control fascicles. A passive chemical cross-linking effect of the inhibitory substances could be excluded by control experiments on devitalized tendon tissue samples (Supplementary figure S7). Based on the additive effect of blocking ROS and MMPs we hypothesized that ROS and MMPs may be hierarchically linked. To address this hypothesis we performed RT-PCR on fascicles cultured in the HiO$_2$HiT+ environment with or without Tempol-treatment blocking ROS. We examined eight genes of interest that had been previously related to proteolysis in our RNAseq results (MMP9, 10 and 13, cathepsin B, C, D, S and Z). Gene expression of MMP9, 10 and cathepsin C was significantly down-regulated by inhibiting ROS with Tempol after 12 days (Figure 5B). A trend towards lower expression of MMP13, cathepsin B and S was observed too. Expression of cathepsins D and Z was not affected by inhibition of ROS. These data show that ROS regulates MMP and cathepsin gene expression directly or indirectly through factors up-stream of nuclear transcription of MMPs.

Taken together, our findings suggest that elevated oxygen and temperature act as pathological drivers of fibroblasts in the tendon core. These cells undergo multifactorial molecular processes that involve oxidative-stress and immune system activation pathways. Inhibiting these pathways was sufficient to abrogate extracellular matrix degradation and functional impairment in unloaded tendon explants.
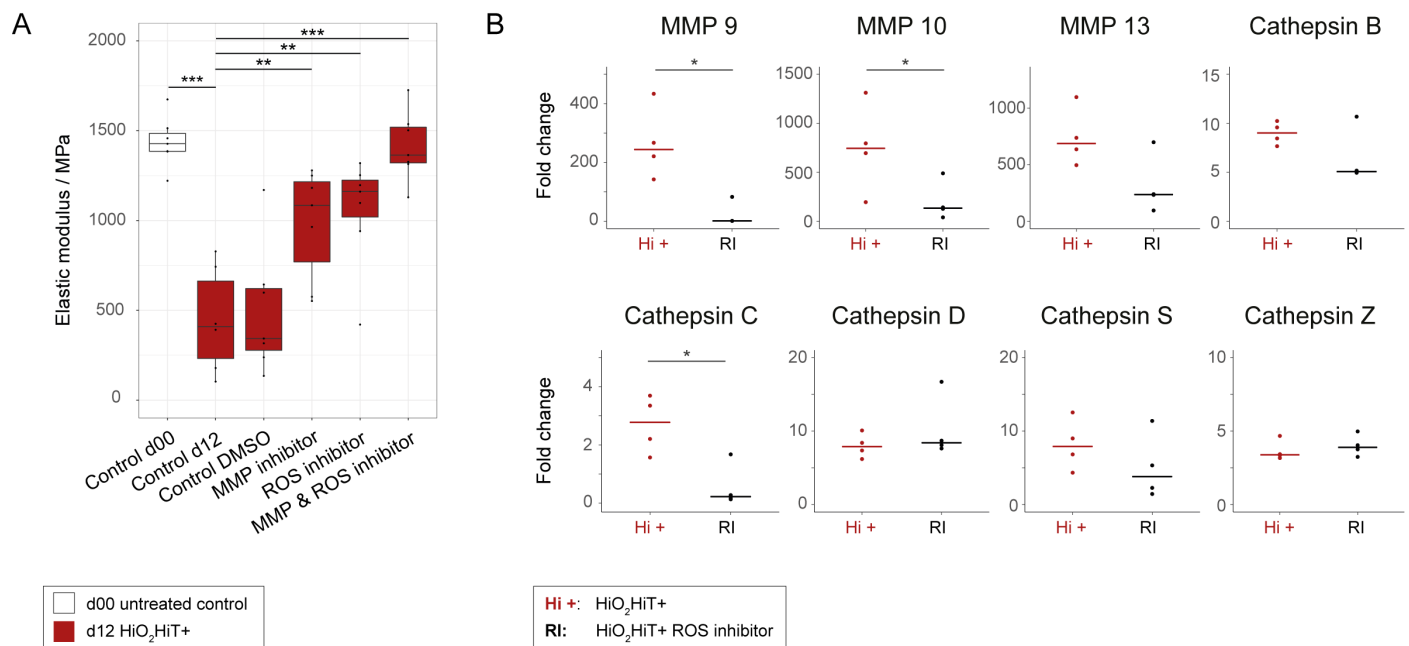
Figure 5: Inhibition of reactive oxygen species (ROS) and MMPs in mechanically impaired tendons. (**A**) Inhibition of ROS and matrix metalloproteinases by Tempol and Ilomastat, respectively. After a culture time of 12 days inhibition of ROS or MMP result in increased elastic modulus compared to the control group. Inhibition of ROS and MMPs show an additive effect restoring original mechanical properties to levels of freshly isolated tissue (Control d0). Statistical analysis was performed using one-way ANOVA followed by contrast analysis in RStudio. Mean values of groups treated with inhibitory substances were compared to the control group cultured for 12 days in serum-supplemented medium (Control d12) (n = 6). (**B**) RT-PCR gene expression of proteins involved in extracellular matrix remodeling after 12 days of culture with and without the ROS inhibitor Tempol. MMP 9, MMP 10 and cathepsin C were significantly down-regulated (p-value = 0.029 for all) in tendon tissue by inhibiting ROS. Gene expression of MMP 13 and cathepsins B, D, S and Z was not significantly affected by ROS inhibition. However a trend of regulation towards native gene expression is observed in MMP 13 and cathepsin B and S. Displayed are the relative fold changes compared to the freshly isolated control at day 0 and the horizontal crossbar represents the median. All values were normalized to the reference gene (Anxa5). Mann-Whitney U tests were performed using in RStudio by comparing the Tempol-supplemented group to the "HiO$_2$HiT+" group (n = 4, p-values: * < 0.05, ** < 0.01, *** < 0.001).

430   Tendon degradome shows altered activity of matrix metalloproteinases and lysosomal proteases

**431   and increased collagen type I cleavage**

432   To quantify proteins and N termini and thereby identify proteolytic cleavage events in intact and

433   degraded tendon explants, we performed 10plex-Tandem Mass Tag^{TM}-Terminal amine isotopic

434   labeling of substrates (TMT-TAILS) (Figure 6A). 382 proteins were quantified with high confidence

435   (FDR < 0.01), of which 35 were significantly more and 13 significantly less (adj. p-value < 0.05; fold

436   change > 1.5) abundant in the degraded HiO$_2$HiT+ phenotype group (Figure 6B, Supplementary table

437   ST4). More abundant hits included proteins associated with proteolysis or lysosomes (MMP3, MMP13,

438   beta-glucuronidase, lysosomal protective protein/cathepsin A, cathepsin Z, V-type proton ATPase

439   subunits A/E1/G1, lysosomal acid phosphatase), intracellular trafficking (sorting nexin 3/5,

440   programmed cell death 6- interacting protein, glycolipid transfer protein) and ROS metabolism

441   (catalase, peroxiredoxin 1). Less abundant proteins are associated with cytoskeletal organization

442   (vimentin, stathmin, cochlin, myocilin, plectin, moesin) or cell-cell and cell-matrix interaction

443   (thrombospondin 1/4).

444   Additionally, we extracted 103 N-terminally TMT-labeled N-terminal semi-tryptic quantifiable

445   peptides from 79 different proteins, whereof 46 could be assigned to curated protein start sites and 57

446   were protease-generated neo-N termini (Figure 6C, Supplementary table ST5). Quantitative N-

447   terminome analysis revealed significantly (adj. p-value < 0.05; fold change > 1.5) increased abundance

448   of active lysosomal proteases (cathepsins B, C, S, Z, lysosomal pepstatin-insensitive protease) all

449   identified by their mature protein N terminus generated upon propeptide removal in the degraded

450   tendon tissue, whereas to our surprise the mature protein N terminus of cathepsin K was inversely

451   abundant between conditions. Transmembrane glycoprotein NMB, which has been identified in

452   osteoclast and macrophage differentiation, was highly abundant in the degraded phenotype and could

453   be determined by a cleavage site within its extracellular domain. Moreover, N-terminomics

454   corroborated increased abundance of MMP13 in the same group, but by identification of a neo-N-

455   terminal peptide, indicating removal of the hemopexin domain with potential implication in altered

456   substrate specificity. Although below the fold-change cut-off of 1.5, we identified 10 collagen type I

457   cleavage sites, of which 8 were significantly more abundant in the mechanically degrading group. Four

458   of these cleavage products were associated with the collagen type I alpha 1 chain (Col1a1) including a

459   known MMP13 site and 4 with the alpha 2 chain (Col1a2).

460   We then quantitatively compared proteins released into supernatants of *ex vivo* tendon cultures under

461   degrading and non-degrading conditions. We identified a total number of 2017 proteins with high

462   confidence (FDR < 0.01) (Supplementary table ST6), of which 351 were only found in the supernatants

463   of the HiO_2HiT+ group (quantifiable in at least two replicates) (e.g. catalase, many proteasome

464   proteins, MMP9 and 24, ADAM10, IL11) and 17 only in the LoO_2LoT+ group. Differential abundance

465   was calculated from 1466 proteins, of which 226 proteins were identified also in the tissue sample

466   (Figure 6D). 740 proteins were significantly more abundant (adj. p-value < 0.05; fold change > 2) in

467   the secretome of the degraded group, accounting for ~85% of all 860 proteins with significantly

468   differential abundance. Quantification of the released proteins corroborated the protease abundance

469   pattern of the tissue proteome showing significantly increased extracellular secretion of proteases, such

470   as cathepsins A, B, D, O, S and MMP13, 14 19, in the degraded group (Figure 6E), while cathepsin K

471   was significantly less abundant in the supernatants of the HiO$_2$HiT+ group.
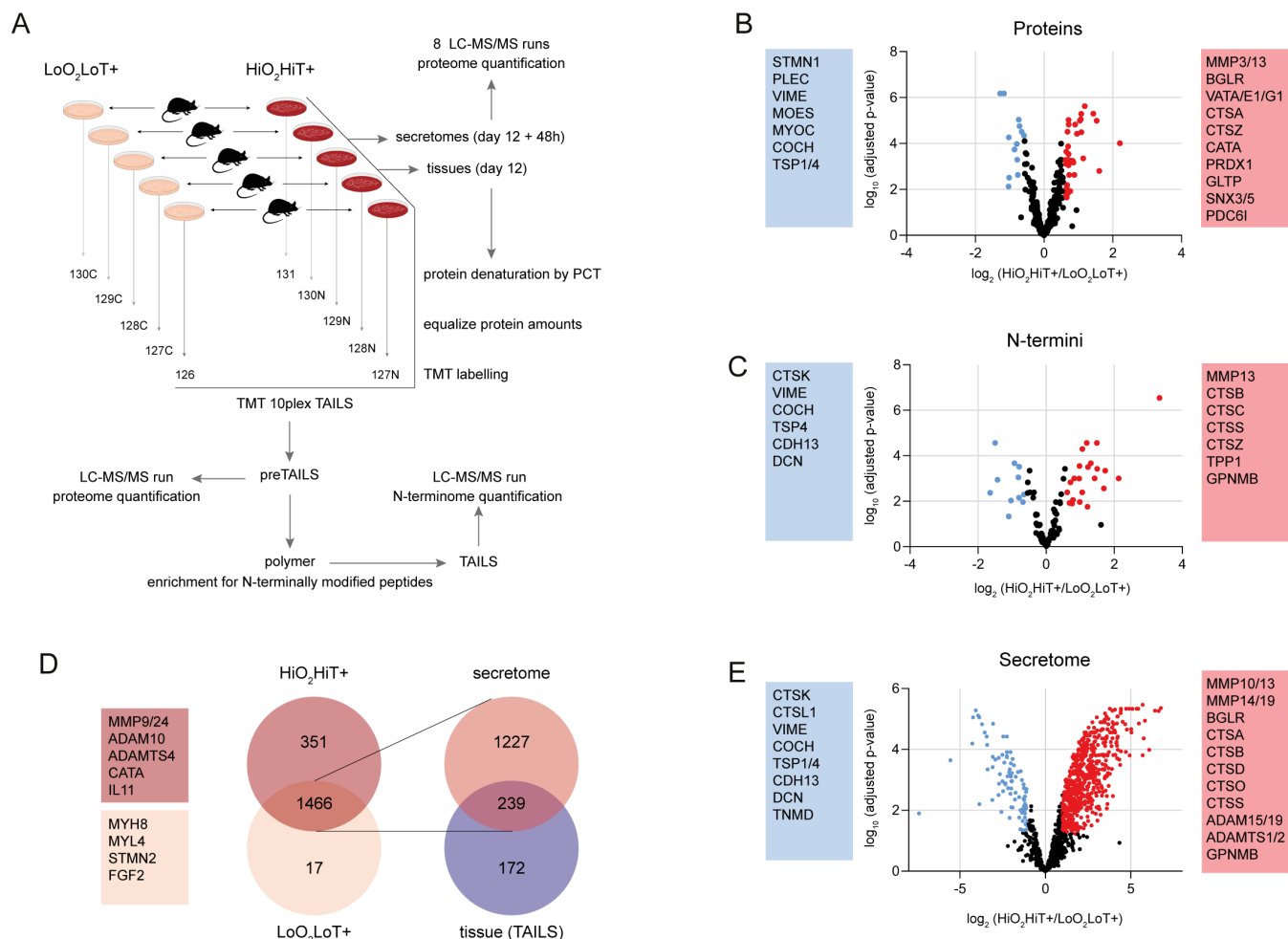
Figure 6: Proteomic analysis mechanically intact and impaired tendon fascicles. (**A**) TMT-TAILS workflow. Tissues of each condition (n=5, independent pools of fascicles from different mice) were collected after 12 days. Protein amounts of all tissue samples were equalized and subsequently analyzed in a 10plex TMT-TAILS experiment. Medium for secretome (n=4) collection was additionally conditioned for 48 hours and analyzed by mass spectrometry based label-free protein quantification method. (**B**) Quantified proteins and (**C**) N termini from TMT-TAILS probes. Proteins coloured in red and blue are considered as differentially more or less abundant and have significance of $p < 0.05$ and a $\log_2$(fold change) > 1.5 (red) or < 1.5 (blue). (**D**) Venn diagram of quantifiable proteins in the secretomes of the mechanically intact (LoO$_2$LoT+) and impaired group (HiO$_2$HiT+). 239 out of totally 1466 secreted proteins were detected both extracellular (released into the medium) and intracellular (tissue, TAILS experiment). (**E**) Label-free quantification of the 1466 secreted proteins of which 860 show significantly different abundance. Red dots (740) show significantly more ($p < 0.05$, $\log_2$(fold change) > 2) and blue dots (120) significantly less ($p < 0.05$, $\log_2$(fold change) < 2) abundant proteins in the HiO$_2$HiT+ group. ADAM = a disintegrin and metalloproteinase, ADAMTS = a disintegrin and metalloproteinase with thrombospondin motif, BGLR = beta-glucuronidase, CATA = catalase, CDH = cadherin, COCH = cochlin, CTS = cathepsin, MMP = matrix metalloproteinase, DCN = decorin, FGF = fibroblast growth factor,

GLTP = glycolipid transfer protein, GPNMB = transmembrane glycoprotein NMB, IL11 = Interleukin 11, MOES = moesin, MYH = myosin, MYL = myosin light chain, MYOC = myocilin, PDC6I = programmed cell death 6-interacting protein, PLEC = plectin, PRDX = peroxiredoxin, SNX = sorting nexin, STMN = stathmin, TNMD = tenomodulin, TPP1 = lysosomal pepstatin-insensitive protease, TSP = thrombospondin, VAT = V-type proton ATPase subunits, VIME = vimentin.

Discussion

Tendon is a tissue with a low innate regenerative capacity, a limited number of resident fibroblasts with normally low metabolic activity, and low tissue vascularity [60, 61]. The mechanisms of tendon remodelling after injury or in chronic tissue pathologies are poorly understood. Observational studies describe the recruitment of cells from the extrinsic tissue compartments (blood vessels, inflammatory mediators) to the tendon core in chronically disordered tendon tissue [39-42]. However, the interplay between the intrinsic tendon core comprised of collagenous ECM and tendon fibroblasts, and the extrinsic peritendinous support tissues during injury and repair remains largely unknown. In this work we studied how the tendon core responds to mechanical load deprivation (that mimics a damage scenario), and how this response may be mediated by presence or lack of a vascularized tissue niche. This question has implications to both understanding chronic tendon disease, and surgical repair of torn tendons.

In this study, tendon microtear with localized matrix unloading was modelled using free-floating culture of murine tail tendon fascicle explants. The fascicle *ex vivo* explant model maintains the cells in their native tissue microenvironment, allows normal cell-cell and cell-matrix communication, and is well suited to the mechanistic study of cell-mediated matrix remodelling in pathophysiological contexts [62-66]. Exploiting this model, we confirmed that standard tissue cultures (elevated nutrient supply, 37°C and 20kPa pO_2) triggered the loss of mechanical properties as shown previously [63, 64, 67, 68]. Strikingly, tendon fascicles that were cultured free-floating with serum at 29°C and 3kPa pO_2 fully maintained their mechanical properties as well as their viability. The additional extrinsic cues of hyperoxia and hyperthermia were required to initiate stromal compartment remodelling. We interpret these cues to represent a vascularized tendon niche, such as expected after severe injury or in advanced stages of tendon disease.

496   After verifying that passive thermodynamic effects of elevated tissue culture on proteolytic kinetics

497   were not responsible for accelerated tissue degradation at higher temperatures [69] (Supplementary

498   figure S3), we investigated the underlying cellular mechanisms. With no obvious differences in macro-

499   nor microscopic tissue structure in conditions to explain the functional loss of tissue strength, we

500   performed a deeper molecular investigation. Comparative quantitative degradomic analysis revealed

501   measurable cleavage of collagen type I in the degraded tissue, consistent with the according loss of

502   macro-mechanical properties. Furthermore, proteomics data showed a general increase in protein

503   release to the supernatant in the functionally impaired group, indicating an elevation in extracellular

504   signalling and secretory capacity under pathological conditions. Activation of cathepsins and MMPs in

505   the degraded phenotype strongly supported the transcriptomic analysis, elaborating in detail the

506   widespread elevation of protease expression. By RNAseq we found that ROS and induction of matrix

507   proteases (MMPs and cathepsins) are linked, which has been widely described earlier in vascular,

508   cardiac, bone and cancer tissues [70-73]. Although ROS have been occasionally mentioned in tendon-

509   related literature their link to protease activation in tendon remodelling processes has been largely

510   overlooked [74-76]. While we can conclude from our data that ROS lay upstream of protease

511   activation, it remains unknown whether hyperthermia and hyperoxia activate a precursor component in

512   the serum that serves as an ignition switch for parallel or consecutive processes, such as ROS

513   generation, tissue degradation and immune system activation. Early research on muscle suggests that

514   hyperthermia induced by exercise directly causes oxidative stress through ROS generation, changes in

515   the immune system and inflammatory response by increased cytokine production [77-79]. According to

516   our RNA-seq dataset it is also conceivable that ROS production and subsequent MMP activation occur

517   via NADPH oxidase. We identified the CYBB gene (also known as NOX2), a member of the NADPH

518   oxidase family, which is described to be present in a large number of tissues including thymus, colon,

519   testis, neurons, skeletal muscle myocytes and endothelial cells, among others [80]. However, it is still

520   widely accepted that CYBB has phagocyte-specific tissue expression. Therefore it seems likely that the

521   cells of the tendon fascicles express a phagocytic-like character. This assumption is further

522   strengthened by the identification of different pathways that are associated with phagocytosis and

523   lysosomes. Phagocytosis is a process of endocytosis when extracellular solid particles are engulfed.

524   The phagosome, the intracellular vacuolar compartment generated during phagocytosis, fuses with the

525   lysosome, an intracellular structure that contains hydrolytic enzymes such as cathepsins, to produce the

526   phagolysosome [81].

527   Furthermore, we identified induced pathways and proteins widely associated with differentiation of

528   osteoclasts, cells closely related to the family of professional phagocytes [82]. Specifically, the up-

529   regulated PPAR gene, which is involved in osteoclast differentiation processes, was recently shown to

530   induce a lysosome-controlled ECM catabolism [83]. In line with these results, matrix resorption in our

531   degraded tendon model might be accelerated by lysosomal proteases upon release from lysosomal

532   vesicles that fuse with the plasma membrane as cathepsins were found both in tissue proteome and

533   secretome [84]. While in bone, cathepsin K is the driving force in ECM degradation, our degradomic

534   data suggest that cathepsins B, C, S and Z are mainly involved in tendon tissue breakdown [85].

535   Interestingly, many cells with a phagocytic character are also the effector cells of the innate immune

536   system thereby acting to enhance inflammation. Likewise, fragments of proteases may also elicit pro-

537   inflammatory signalling [86-88]. Therefore, it is tempting to speculate that phagocytosed ECM

538   components are cleaved by proteases within the lysosome and the generated fragments may

539   subsequently serve as mediators of inflammation and immune response as so called damage-associated

540   molecular patterns (DAMPs) [89-91]. DAMPs are known to initiate a non-infectious inflammatory

541   response by activating antigen-presenting cells to become stimulatory to the adaptive immune system

542   [92, 93].

543   Taken together, exogenous peptides generated from extracellular matrix breakdown after acute loss of

544   mechanical tension in a pathological tissue may be internalized by phagocytosis, processed in the

545   phagolysosome to produce fragments that serve as "antigens", which are finally presented to the

546   immune system via class I MHC (also found induced in our RNA-seq data) in tendon fibroblasts. This

547   process, also known as cross-presentation [94], has been identified as the most significantly regulated

548   pathway in our impaired tendon model. It may be that a small fraction of cleaved matrix fragments

549   remain to act as DAMPs, while the majority is eventually recycled into the functional matrix. This

550   concept of recycling of ECM proteins during remodelling is supported by evidence that *de novo*

551   synthesis of ECM in healthy tendon appears to be very limited over the course of an individual lifetime

552   [95].

553   Among the limitations of the present work is that it only captures unidirectional extrinsic gating of the

554   intrinsic compartment, neglecting bidirectional signaling between the intrinsic and extrinsic tissue

555   compartments. Interpreting how signals released into the extracellular microenvironment act on cells

556   and ECM might be instructive for further deciphering the communication between tissue compartments

557   in the context of immune response, for better understanding the pathological mechanisms and revealing

558   a possible phenotype shift of cells within the native tissue.

559   Overall our data demonstrate that tissue temperature and oxygen levels represent decisive contextual

560   cues in triggering ECM proteolysis after mechanical unloading. Hyperoxic and hyperthermic

561   conditions mimic pathological vascularity, and apparently act as a gate to the onset of catabolic tissue

562   turnover. The involved pathways include ROS, protease induction and immune-cell recruitment. Our

563   data provide key insights into how initially quiescent tendon cells are activated to work as executers of

564   tissue remodelling in the absence of active extrinsic helper cells. A major aspect of our work is that it

565   highlights the physiological role of low oxygen and below body core temperatures as important in

566   maintaining cellular quiescence and functional integrity of the ECM. Mechanical tension is

567   dogmatically considered to be essential to protect tendon tissue from proteolytic turnover and tissue

568   remodelling. It is therefore remarkable that mechanics alone were insufficient to trigger proteolytic

569   matrix turnover in low oxygen and temperature. Among other implications, our findings suggest that

570   tendon cell and tissue culture conditions should be reconsidered in experimental settings that study

571   healthy tissue. This does not only apply for the tendon field but also for scientific investigations of

572   other stromal tissues with normally low vascularity, such as cartilage, the intervertebral discs and

573   ligaments.

574   We present a tendon *ex vivo* model that by changing the culture environment can be used to reflect

575   tendon physiology or pathophysiology. To our knowledge this is the first study to in-depth investigate

576   the events leading to tissue degradation at the tissue (biomechanics, tissue morphology, cell viability)

577   and molecular level (transcriptomics and degradomics) and thereby offering broad insight into how

578   multifactorial molecular processes may converge to a possible mechanism, by which ECM homeostasis

579   is shifted towards degradation. Collectively, we anticipate that our study will have a significant impact

580   in the field of tendon biology by contributing to a more mechanistic understanding of tendon

581   physiology and at the same time helping to effectively progress the development of effective treatments

582   for tendinopathy. Furthermore, our observations give rise to many new hypotheses for future

583   investigations involving ECM remodelling, oxidative stress and immune-related cellular response in

584   tendon and stromal tissue.

585 **Acknowledgment**

References

1.   Lee, A.H. and D.M. Elliott, *Comparative multi-scale hierarchical structure of the tail, plantaris, and Achilles tendons in the rat.* J Anat, 2018.

2.   O'Brien, M., *Structure and metabolism of tendons.* Scand J Med Sci Sports, 1997. **7**(2): p. 55-61.

3.   Handsfield, G.G., L.C. Slane, and H.R. Screen, *Nomenclature of the tendon hierarchy: An overview of inconsistent terminology and a proposed size-based naming scheme with terminology for multi-muscle tendons.* J Biomech, 2016.

4.   Reeves, N.D., C.N. Maganaris, and M.V. Narici, *Effect of strength training on human patella tendon mechanical properties of older individuals.* J Physiol, 2003. **548**(Pt 3): p. 971-81.

5.   Maganaris, C.N., et al., *Adaptive response of human tendon to paralysis.* Muscle Nerve, 2006. **33**(1): p. 85-92.

6.   Rosager, S., et al., *Load‐displacement properties of the human triceps surae aponeurosis and tendon in runners and non‐runners.* Scandinavian journal of medicine & science in sports, 2002. **12**(2): p. 90-98.

7.   Khayyeri, H., et al., *Achilles tendon compositional and structural properties are altered after unloading by botox.* Sci Rep, 2017. **7**(1): p. 13067.

8.   Marqueti, R.C., et al., *Effects of aging and resistance training in rat tendon remodeling.* FASEB J, 2018. **32**(1): p. 353-368.

9.   Soslowsky, L.J., et al., *Neer Award 1999: Overuse activity injures the supraspinatus tendon in an animal model: A histologic and biomechanical study.* Journal of Shoulder and Elbow Surgery, 2000. **9**(2): p. 79-84.

10.   Knobloch, K., U. Yoon, and P.M. Vogt, *Acute and overuse injuries correlated to hours of training in master running athletes.* Foot Ankle Int, 2008. **29**(7): p. 671-6.

11.   Spiesz, E.M., et al., *Tendon extracellular matrix damage, degradation and inflammation in response to in-vitro overload exercise.* J Orthop Res, 2015.

12.   Thorpe, C.T., et al., *Tendon overload results in alterations in cell shape and increased markers of inflammation and matrix degradation.* Scandinavian Journal of Medicine & Science in Sports, 2015: p. n/a-n/a.

13.   McCormick, A., J. Charlton, and D. Fleming, *Assessing health needs in primary care. Morbidity study from general practice provides another source of information.* BMJ: British Medical Journal, 1995. **310**(6993): p. 1534.

14.   Andarawis-Puri, N., E.L. Flatow, and L.J. Soslowsky, *Tendon basic science: Development, repair, regeneration, and healing.* J Orthop Res, 2015. **33**(6): p. 780-4.

15.   Docheva, D., et al., *Biologics for tendon repair.* Adv Drug Deliv Rev, 2015. **84**: p. 222-39.

16.   Millar, N.L., G.A. Murrell, and I.B. McInnes, *Inflammatory mechanisms in tendinopathy - towards translation.* Nat Rev Rheumatol, 2017. **13**(2): p. 110-122.

17.   Cook, J.L. and C.R. Purdam, *Is tendon pathology a continuum? A pathology model to explain the clinical presentation of load-induced tendinopathy.* Br J Sports Med, 2009. **43**(6): p. 409-16.

18.   Cook, J.L., et al., *Revisiting the continuum model of tendon pathology: what is its merit in clinical practice and research?* Br J Sports Med, 2016. **50**(19): p. 1187-91.

19.   Abate, M., et al., *Pathogenesis of tendinopathies: inflammation or degeneration?* Arthritis research & therapy, 2009. **11**(3): p. 235.

20.   Arnoczky, S.P., M. Lavagnino, and M. Egerbacher, *The mechanobiological aetiopathogenesis of tendinopathy: is it the over-stimulation or the under-stimulation of tendon cells?* Int J Exp Pathol, 2007. **88**(4): p. 217-26.

21.   Lin, T.W., L. Cardenas, and L.J. Soslowsky, *Biomechanics of tendon injury and repair.* J Biomech, 2004. **37**(6): p. 865-77.

22.   Pelled, G., et al., *Smad8/BMP2-engineered mesenchymal stem cells induce accelerated recovery of the biomechanical properties of the Achilles tendon.* J Orthop Res, 2012. **30**(12): p. 1932-9.

23.   Riggin, C.N., T.R. Morris, and L.J. Soslowsky, *Tendinopathy II: Etiology, Pathology, and healing of Tendon Injury and Disease*, in *Tendon Regeneration*. 2015, Elsevier. p. 149-183.

24.   Xu, Y. and G.A. Murrell, *The basic science of tendinopathy.* Clin Orthop Relat Res, 2008. **466**(7): p. 1528-38.

25.   Kragsnaes, M.S., et al., *Stereological quantification of immune-competent cells in baseline biopsy specimens from achilles tendons: results from patients with chronic tendinopathy followed for more than 4 years.* Am J Sports Med, 2014. **42**(10): p. 2435-45.

26.   Dakin, S.G., et al., *Chronic inflammation is a feature of Achilles tendinopathy and rupture.* Br J Sports Med, 2018. **52**(6): p. 359-367.

27.   Rees, J.D., M. Stride, and A. Scott, *Tendons--time to revisit inflammation.* Br J Sports Med, 2014. **48**(21): p. 1553-7.

28.   Ackermann, P.W., et al., *Neuronal pathways in tendon healing and tendinopathy–update.* Front Biosci (Landmark Ed), 2014. **19**: p. 1251-78.

29.   Arya, S. and K. Kulig, *Tendinopathy alters mechanical and material properties of the Achilles tendon.* J Appl Physiol (1985), 2010. **108**(3): p. 670-5.

30.   Seto, S.P., et al., *Cathepsins in Rotator Cuff Tendinopathy: Identification in Human Chronic Tears and Temporal Induction in a Rat Model.* Ann Biomed Eng, 2015. **43**(9): p. 2036-46.

31.   Riley, G.P., et al., *Matrix metalloproteinase activities and their relationship with collagen remodelling in tendon pathology.* Matrix Biology, 2002. **21**(2): p. 185-195.

32.   Smith, M.M., et al., *Modulation of aggrecan and ADAMTS expression in ovine tendinopathy induced by altered strain.* Arthritis Rheum, 2008. **58**(4): p. 1055-66.

33.   Dyment, N.A., et al., *The paratenon contributes to scleraxis-expressing cells during patellar tendon healing.* PLoS One, 2013. **8**(3): p. e59944.

34.   Cadby, J.A., et al., *Differences between the cell populations from the peritenon and the tendon core with regard to their potential implication in tendon repair.* PLoS One, 2014. **9**(3): p. e92474.

35.   Mienaltowski, M.J., S.M. Adams, and D.E. Birk, *Regional differences in stem cell/progenitor cell populations from the mouse achilles tendon.* Tissue Eng Part A, 2013. **19**(1-2): p. 199-210.

36.   Howell, K., et al., *Novel Model of Tendon Regeneration Reveals Distinct Cell Mechanisms Underlying Regenerative and Fibrotic Tendon Healing.* Sci Rep, 2017. **7**: p. 45238.

37.   Tempfer, H. and A. Traweger, *Tendon Vasculature in Health and Disease.* Front Physiol, 2015. **6**: p. 330.

38.   Snedeker, J.G. and J. Foolen, *Tendon injury and repair - A perspective on the basic mechanisms of tendon disease and future clinical therapy.* Acta Biomater, 2017.

39.   Järvinen, M., et al., *Histopathological findings in chronic tendon disorders.* Scandinavian Journal of Medicine & Science in Sports, 1997. **7**(2): p. 86-95.

40.   Ohberg, L., R. Lorentzon, and H. Alfredson, *Neovascularisation in Achilles tendons with painful tendinosis but not in normal tendons: an ultrasonographic investigation.* Knee Surg Sports Traumatol Arthrosc, 2001. **9**(4): p. 233-8.

41.   Scott, A., E. Huisman, and K. Khan, *Conservative treatment of chronic Achilles tendinopathy.* Canadian Medical Association Journal, 2011. **183**(10): p. 1159-1165.

42.   Alfredson, H., L. Ohberg, and S. Forsgren, *Is vasculo-neural ingrowth the cause of pain in chronic Achilles tendinosis? An investigation using ultrasonography and colour Doppler, immunohistochemistry, and diagnostic injections.* Knee Surg Sports Traumatol Arthrosc, 2003. **11**(5): p. 334-8.

43.   Wunderli, S.L., et al., *Minimal mechanical load and tissue culture conditions preserve native cell phenotype and morphology in tendon-a novel ex vivo mouse explant model.* J Orthop Res, 2018. **36**(5): p. 1383-1390.

44.   Hatakeyama, M., et al., *SUSHI: an exquisite recipe for fully documented, reproducible and reusable NGS data analysis.* BMC bioinformatics, 2016. **17**(1): p. 228.

45.   Dobin, A., et al., *STAR: ultrafast universal RNA-seq aligner.* Bioinformatics, 2013. **29**(1): p. 15-21.

46.   Liao, Y., G.K. Smyth, and W. Shi, *featureCounts: an efficient general purpose program for assigning sequence reads to genomic features.* Bioinformatics, 2013. **30**(7): p. 923-930.

47.   Love, M.I., W. Huber, and S. Anders, *Moderated estimation of fold change and dispersion for RNA-seq data with DESeq2*. Genome Biol, 2014. **15**(12): p. 550.

48.   Young, M.D., et al., *Gene ontology analysis for RNA-seq: accounting for selection bias.* Genome biology, 2010. **11**(2): p. R14.

49.   Falcon, S. and R. Gentleman, *Using GOstats to test gene lists for GO term association.* Bioinformatics, 2007. **23**(2): p. 257-8.

50.   Conesa, A., et al., *A survey of best practices for RNA-seq data analysis.* Genome Biol, 2016. **17**: p. 13.

51.   Schmittgen, T.D. and K.J. Livak, *Analyzing real-time PCR data by the comparative C(T) method.* Nat Protoc, 2008. **3**(6): p. 1101-8.

52.   Madzharova, E., F. Sabino, and U. auf dem Keller, *Exploring Extracellular Matrix Degradomes by TMT-TAILS N-Terminomics*, in *Collagen*. 2019, Springer. p. 115-126.

53.   Kleifeld, O., et al., *Identifying and quantifying proteolytic events and the natural N terminome by terminal amine isotopic labeling of substrates.* Nat Protoc, 2011. **6**(10): p. 1578-611.

54.   Rainer, J., et al., *CARMAweb: comprehensive R-and bioconductor-based web service for microarray data analysis.* Nucleic acids research, 2006. **34**(suppl_2): p. W498-W503.

55.   Fortelny, N., et al., *Proteome TopFIND 3.0 with TopFINDer and PathFINDer: database and analysis tools for the association of protein termini to pre- and post-translational events.* Nucleic Acids Res, 2015. **43**(Database issue): p. D290-7.

56.   R Core Team, *R: A language and environment for statistical computing*. 2013, R Foundation for Statistical Computing: Vienna, Austria.

57.   Carreau, A., et al., *Why is the partial oxygen pressure of human tissues a crucial parameter? Small molecules and hypoxia.* J Cell Mol Med, 2011. **15**(6): p. 1239-53.

58.   Kubo, K., et al., *Noninvasive measures of blood volume and oxygen saturation of human Achilles tendon by red laser lights.* Acta Physiol (Oxf), 2008. **193**(3): p. 257-64.

59.   Berge, O.-G., I. Garcia-Cabrera, and K. Hole, *Response latencies in the tail-flick test depend on tail skin temperature.* Neuroscience Letters, 1988. **86**(3): p. 284-288.

60.   Pufe, T., et al., *Mechanical factors influence the expression of endostatin—an inhibitor of angiogenesis—in tendons.* Journal of orthopaedic research, 2003. **21**(4): p. 610-616.

61.   Rees, J.D., A.M. Wilson, and R.L. Wolman, *Current concepts in the management of tendon disorders.* Rheumatology (Oxford), 2006. **45**(5): p. 508-21.

62.   Arnoczky, S., et al., *Ex vivo static tensile loading inhibits MMP-1 expression in rat tail tendon cells through a cytoskeletally based mechanotransduction mechanism.* Journal of Orthopaedic Research, 2004. **22**(2): p. 328 - 333.

63.   Arnoczky, S.P., et al., *Matrix metalloproteinase inhibitors prevent a decrease in the mechanical properties of stress-deprived tendons: an in vitro experimental study.* Am J Sports Med, 2007. **35**(5): p. 763-9.

64.   Abreu, E.L., D. Leigh, and K.A. Derwin, *Effect of altered mechanical load conditions on the structure and function of cultured tendon fascicles.* J Orthop Res, 2008. **26**(3): p. 364-73.

65.   Cousineau-Pelletier, P. and E. Langelier, *Relative contributions of mechanical degradation, enzymatic degradation, and repair of the extracellular matrix on the response of tendons when subjected to under- and over- mechanical stimulations in vitro.* J Orthop Res, 2010. **28**(2): p. 204-10.

66.   Screen, H.R., et al., *The influence of noncollagenous matrix components on the micromechanical environment of tendon fascicles.* Ann Biomed Eng, 2005. **33**(8): p. 1090-9.

67.   Hannafin, J.A., et al., *Effect of stress deprivation and cyclic tensile loading on the material and morphologic properties of canine flexor digitorum profundus tendon: An in vitro study.* Journal of Orthopaedic Research, 1995. **13**(6): p. 907-914.

68.   Wang, T., et al., *Cyclic mechanical stimulation rescues Achilles tendon from degeneration in a bioreactor system.* Journal of Orthopaedic Research, 2015: p. n/a-n/a.

69.   Fasciglione, G.F., et al., *pH-and temperature-dependence of functional modulation in metalloproteinases. A comparison between neutrophil collagenase and gelatinases A and B.* Biophysical journal, 2000. **79**(4): p. 2138-2149.

70.   Rajagopalan, S., et al., *Reactive Oxygen Species Produced by Macrophage-derived Foam Cells Regulate the Activity of Vascular Matrix Metalloproteinases In Vitro.* JOURNAL OF CLINICAL INVESTIGATION 1996. **98**(11): p. 2572-2579.

71.   Siwik, D.A., P.J. Pagano, and W.S. Colucci, *Oxidative stress regulates collagen synthesis and matrix metalloproteinase activity in cardiac fibroblasts.* American Journal of Physiology-Cell Physiology, 2001. **280**(1): p. C53-C60.

72.   Ramamurthy, N.S., et al., *Reactive oxygen species activate and tetracyclines inhibit rat osteoblast collagenase.* Journal of Bone and Mineral Research, 1993. **8**(10): p. 1247-1253.

73.   Hsieh, C.L., et al., *Reactive oxygen species-mediated switching expression of MMP-3 in stromal fibroblasts and cancer cells during prostate cancer progression.* Sci Rep, 2017. **7**(1): p. 9065.

74.   Bestwick, C. and N. Maffulli, *Reactive oxygen species and tendinopathy: do they matter?* British journal of sports medicine, 2004. **38**(6): p. 672-674.

75.   Longo, U.G., et al., *Oxygen species and overuse tendinopathy in athletes.* Disabil Rehabil, 2008. **30**(20-22): p. 1563-71.

76.   Wang, F., G.A. Murrell, and M.X. Wang, *Oxidative stress-induced c-Jun N-terminal kinase (JNK) activation in tendon cells upregulates MMP1 mRNA and protein expression.* J Orthop Res, 2007. **25**(3): p. 378-89.

77.   Pedersen, B.K. and L. Hoffman-Goetz, *Exercise and the immune system: regulation, integration, and adaptation.* Physiological reviews, 2000. **80**(3): p. 1055-1081.

78.   Peake, J., K.K. Nosaka, and K. Suzuki, *Characterization of inflammatory responses to eccentric exercise in humans.* 2005.

79.   Salo, D.C., C.M. Donovan, and K.J. Davies, *HSP70 and other possible heat shock or oxidative stress proteins are induced in skeletal muscle, heart, and liver during exercise.* Free Radical Biology and Medicine, 1991. **11**(3): p. 239-246.

80.   Bedard, K. and K.-H. Krause, *The NOX family of ROS-generating NADPH oxidases: physiology and pathophysiology.* Physiological reviews, 2007. **87**(1): p. 245-313.

81.   Klionsky, D.J., E.L. Eskelinen, and V. Deretic, *Autophagosomes, phagosomes, autolysosomes, phagolysosomes, autophagolysosomes... wait, I'm confused.* Autophagy, 2014. **10**(4): p. 549-51.

82.   Gordon, S., *Phagocytosis: An Immunobiologic Process.* Immunity, 2016. **44**(3): p. 463-475.

83.   Zhao, X., et al., *Metabolic regulation of dermal fibroblasts contributes to skin extracellular matrix homeostasis and fibrosis.* Nature Metabolism, 2019. **1**(1): p. 147-157.

84.   Tu, C., et al., *Lysosomal cathepsin B participates in the podosome-mediated extracellular matrix degradation and invasion via secreted lysosomes in v-Src fibroblasts.* Cancer Res, 2008. **68**(22): p. 9147-56.

85.   Teitelbaum, S.L., *Bone resorption by osteoclasts.* Science, 2000. **289**(5484): p. 1504-1508.

86.   Parks, W.C., C.L. Wilson, and Y.S. Lopez-Boado, *Matrix metalloproteinases as modulators of inflammation and innate immunity.* Nat Rev Immunol, 2004. **4**(8): p. 617-29.

87.   Wiedow, O. and U. Meyer‐Hoffert, *Neutrophil serine proteases: potential key regulators of cell signalling during inflammation.* Journal of internal medicine, 2005. **257**(4): p. 319-328.

88.   Khokha, R., A. Murthy, and A. Weiss, *Metalloproteinases and their natural inhibitors in inflammation and immunity.* Nat Rev Immunol, 2013. **13**(9): p. 649-65.

89.   Thomas, A.H., E.R. Edelman, and C.M. Stultz, *A brief communication: Collagen Fragments Modulate Innate Immunity.* Experimental Biology and Medicine, 2007. **232**(3): p. 406-411.

90.   Adair-Kirk, T.L. and R.M. Senior, *Fragments of extracellular matrix as mediators of inflammation.* Int J Biochem Cell Biol, 2008. **40**(6-7): p. 1101-10.

91.   Sorokin, L., *The impact of the extracellular matrix on inflammation.* Nat Rev Immunol, 2010. **10**(10): p. 712-23.

92.   Kono, H. and K.L. Rock, *How dying cells alert the immune system to danger.* Nat Rev Immunol, 2008. **8**(4): p. 279-89.

93.   De Lorenzo, G., et al., *Extracellular DAMPs in Plants and Mammals: Immunity, Tissue Damage and Repair.* Trends Immunol, 2018. **39**(11): p. 937-950.

94.   Burgdorf, S. and M. Embgenbroich, *Current concepts of antigen cross-presentation.* Frontiers in immunology, 2018. **9**: p. 1643.

95.   Heinemeier, K.M., et al., *Lack of tissue renewal in human adult Achilles tendon is revealed by nuclear bomb (14)C.* FASEB J, 2013. **27**(5): p. 2074-9.

Supplementary figures
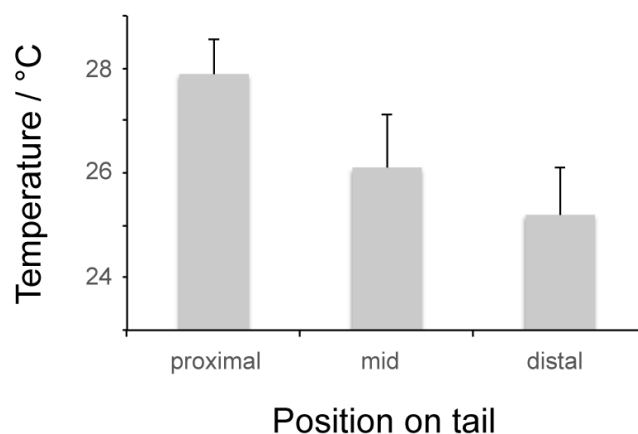
Figure S1: Superficial temperature of the mouse tail was estimated by measuring infrared emission at different locations. Skin temperature decreases with increasing distance to the body core. The tail of rodents is thought to act as a temperature regulator. Heat is brought by the blood flow through the central tail artery and is dissipated through the skin. The columns represent mean values and the error bars standard deviation (n = 40).
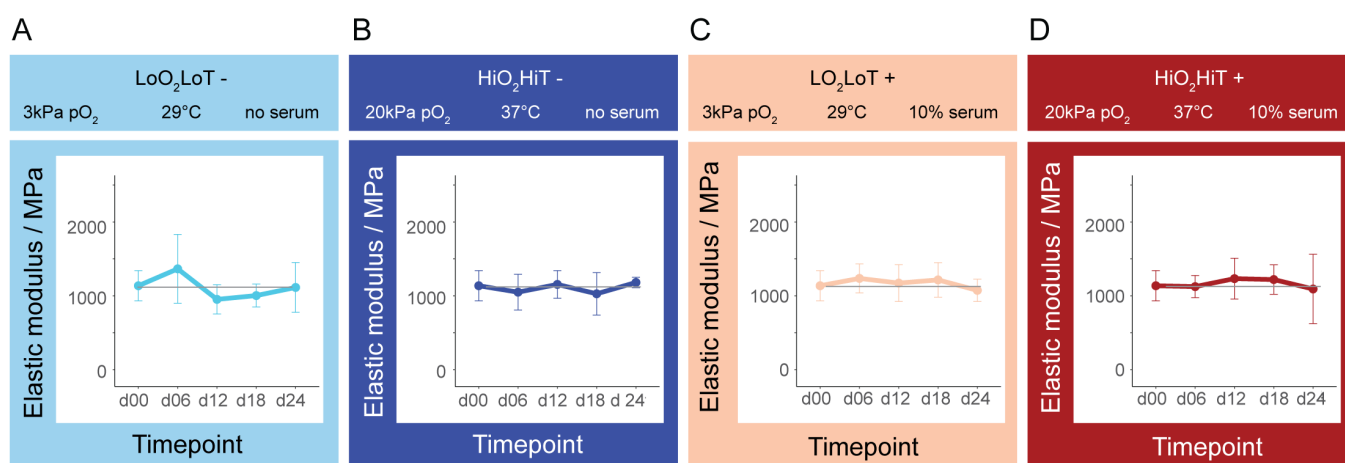

Figure S2: Elastic moduli of devitalized tendon fascicles cultured in the different environments over a time period of 24 days (d24). The data points represent mean values and the error bars represent standard deviation. Statistical analysis was performed using one-way ANOVA with a contrast matrix in RStudio. Mean values of each time-point (d06 – d24) were compared to the freshly isolated control (d00) within each condition (n = 6 independent samples from different mice).
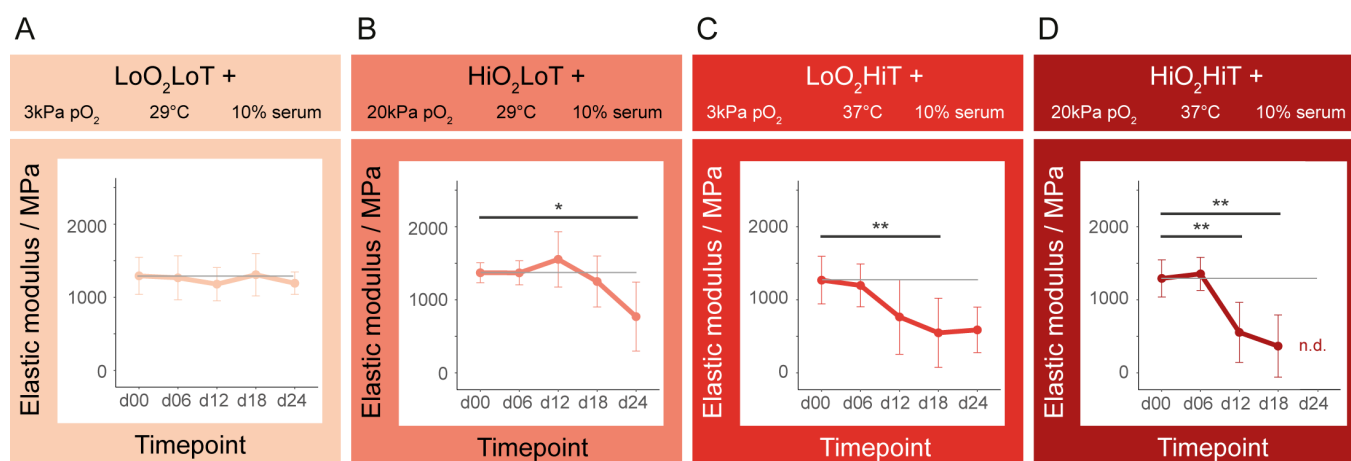
Figure S3: Elastic moduli of tendon fascicles cultured in different environments during 24 days (d24). The models represent extrinsic compartment involvement with progressive increase in severity (**A** to **D**). The additional culture conditions were introduced to better understand the quasi-decoupled effect of high temperature or high oxygen on extracellular matrix degradation. The data points represent mean values and the error bars are standard deviation. Statistical analysis was performed using one-way ANOVA followed by contrast analysis in RStudio. Mean values of each time-point (d06 – d24) were compared to the freshly isolated control (d00) within each condition (n = 6 independent samples from different mice, p-values: * < 0.05, ** < 0.01).
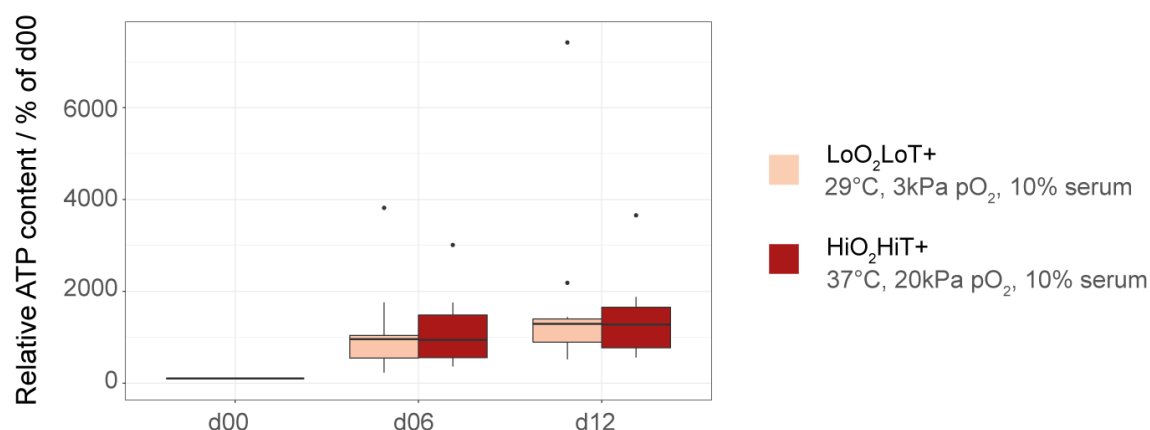

Figure S4: Normalized ATP content of mechanically intact and degraded tendon fascicles. Normalized ATP content was comparable between groups at each timepoint (d06 and d12). Boxplots display median value and $1^{st}/3^{rd}$ quartiles. Outliers are plotted as individual data points. Three outliers > 7500 were removed. Statistical analysis was performed using Mann-Whitney U test in RStudio comparing the "LoO$_2$LoT+" to the "HiO$_2$HiT+" condition within each time point. (n = 4 in duplicates, with two measurements per animal).
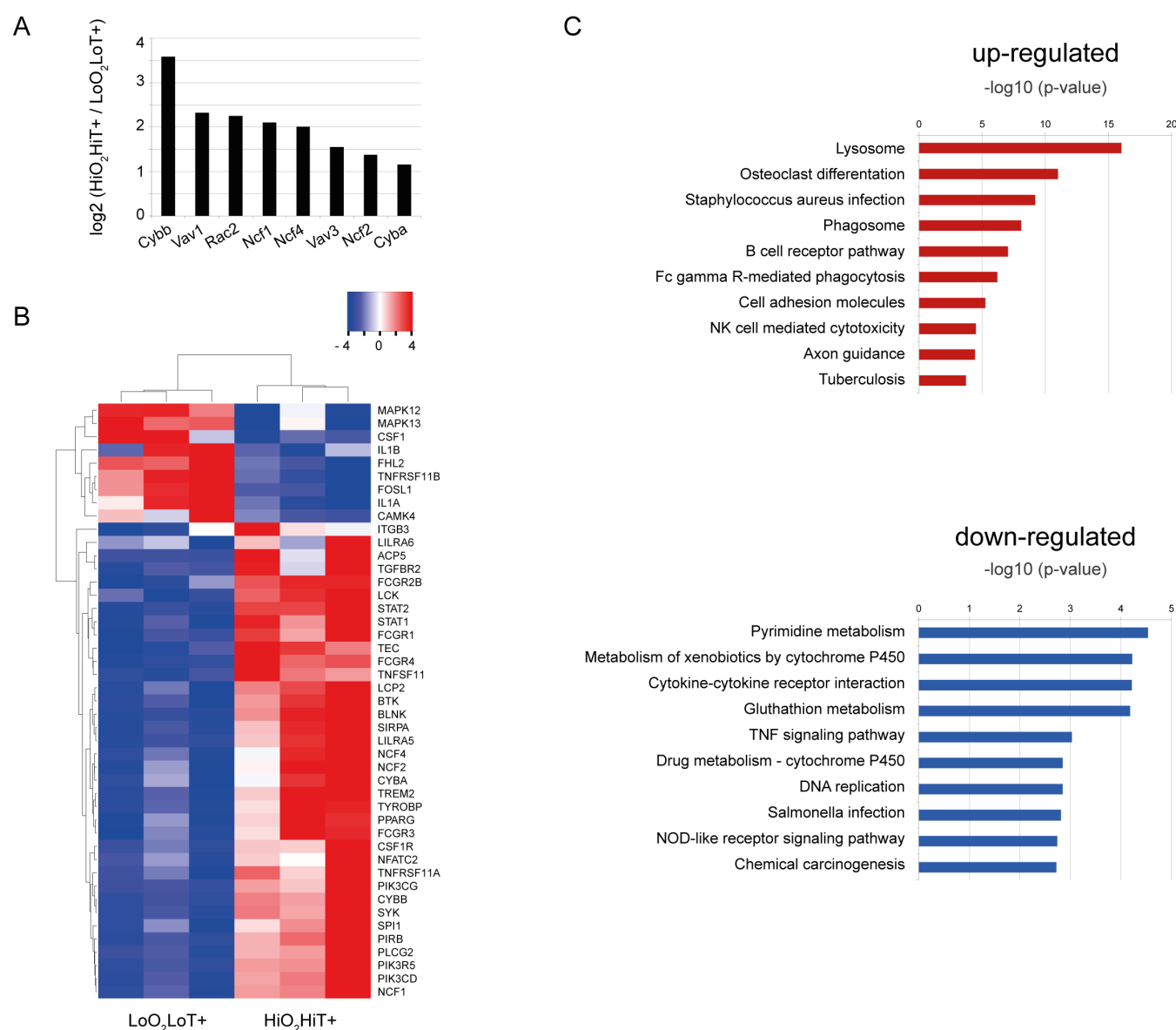
Figure S5: RNA-seq data analysis of differentially expressed genes comparing mechanically intact and degraded tendon fascicles. (**A**) All genes associated with NADPH oxidase are significantly up-regulated in the functionally impaired group (HiO$_2$HiT+). Represented are the significantly differentially expressed genes with a log2 ratio of > 1 and a p-value < 0.05. (**B**) Heatmap of genes mapped to the KEGG pathway "Osteoclast differentiation". The cluster separates the differentially expressed genes by colour with positive or negative row-scaled Z-scores represented in red and blue, respectively. (**C**) The top 10 enriched signalling pathways in the HiO$_2$HiT+ group compared to the LoO$_2$LoT+ group determined by the KEGG database separated by up- and down-regulated genes.
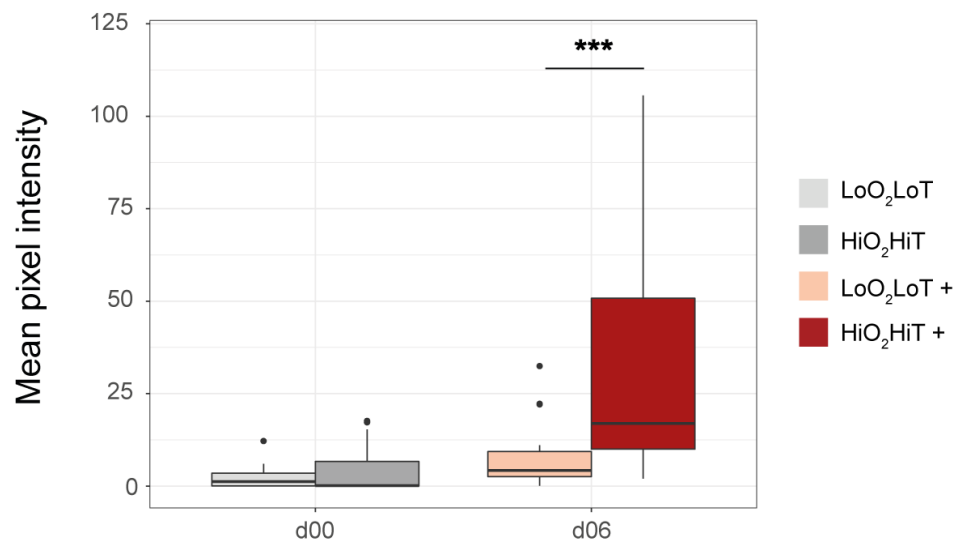
Figure S6: Detection of reactive oxygen species (ROS) by quantification of fluorescence intensity of DCF in tendon fascicles upon incubation at either 29°C and 3kPa pO_2 (LoO_2LoT) or 37°C and 203kPa pO_2 (HiO_2HiT) for 30min directly after extraction from the tail (d00) or after incubation in serum containing medium (+) in LoO_2LoT or HiO_2HiT environment for 6 days. Boxplots display median value and $1^{st}/3^{rd}$ quartiles. Mann-Whitney U test (RStudio) was used to probe statistically significant differences between the LoO_2LoT and HiO_2HiT condition within each time point. (n = 6, *** < 0.001). Presence of ROS was significantly different between the two culture environments at day 6 (p-value = 0.0004).
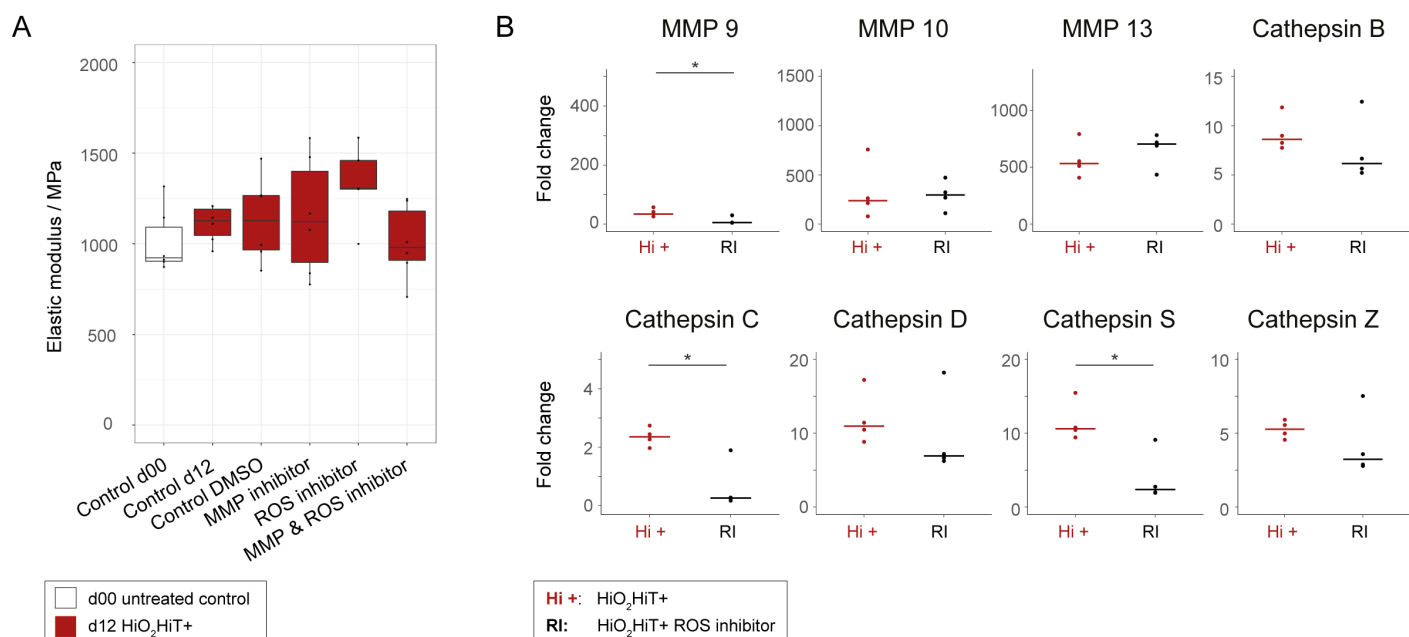
Figure S7: Pharmacological inhibition experiments on mechanically degrading tendon fascicles. (**A**) Elastic moduli of devitalized tissue cultured with different inhibitors at 37°C, 20kPa pO_2 in 10% serum for 12 days. The elastic modulus is not significantly different between the conditions (n=7). Statistical analysis was performed using one-way ANOVA followed by contrast analysis in RStudio. Mean values of groups treated with inhibitory substances were compared to the control group cultured for 12 days in serum-supplemented medium (Control d12) (n = 7). (**B**) RT-PCR gene expression of proteins involved in extracellular matrix remodeling after 6 days of culture with and without the ROS inhibitor Tempol. MMP 9, cathepsins C and S are significantly down-regulated (p-value = 0.029) in tendon tissue by inhibiting ROS. Gene expression of MMP 10, 13 and cathepsins B, D and Z was not significantly affected by ROS inhibition. Displayed are the relative fold changes compared to the freshly isolated control at d00 and the horizontal crossbar represents the median. All values were normalized to the reference gene (Anxa5). Mann-Whitney U tests were performed using in RStudio by comparing the Tempol-supplemented group to the "HiO$_2$HiT+" group (n = 4, p-values: * < 0.05).